BIOGENIC SYNTHESIS OF NICKEL OXIDE NANOPARTICLES USING *FICUS RELIGIOSA* AND THEIR APPLICATION TO SEQUESTRATE ANIONIC DYE

Dissertation Submitted
In Partial Fulfilment of the Requirements for the
Degree of

Master of Science (M.Sc.)

in

CHEMISTRY

By

HARSHITA THAPA
(2K24/MSCCHE/31)

JYOTI TOMAR
(2K24/MSCCHE/51)

Under the supervision of
Prof. ANIL KUMAR

Department of Applied Chemistry

DELHI TECHNOLOGICAL UNIVERSITY
(Formerly Delhi College of Engineering)
Shahbad Daulatpur, Main Bawana Road, Delhi-110042

June, 2026

DELHI TECHNOLOGICAL UNIVERSITY
(Formerly Delhi College of Engineering)
Shahbad Daulatpur, Main Bawana Road, Delhi-42

ACKNOWLEDGEMENT

The success of this project was made possible with the invaluable guidance and assistance from many individuals.

We express our sincere gratitude to our project supervisor, **Prof. Anil Kumar**, Department of Applied Chemistry, Delhi Technological University, for his invaluable guidance, constant encouragement and mentorship throughout the project. A special thanks to Ph.D. scholar **Dr. Priyanka Yadav** for her continuous support, valuable suggestions, and unwavering motivation throughout the course of this work. We are grateful to the entire teaching and non-teaching staff of the Department for their constant encouragement, support, and guidance during this project. Lastly, we extend our heartfelt gratitude to our beloved family and friends for their unwavering support and motivation, which kept us going through the long working hours.

HARSHITA THAPA
2K24/MSCCHE/31

JYOTI TOMAR
2K24/MSCCHE/51

DELHI TECHNOLOGICAL UNIVERSITY
(Formerly Delhi College of Engineering)
Shahbad Daulatpur, Main Bawana Road, Delhi-42

DECLARATION

We, **HARSHITA THAPA** & **JYOTI TOMAR**, hereby declare that the work which is being submitted in this dissertation entitled "**Biogenic Synthesis of NiO Nanoparticles using *Ficus Religiosa* and their application to Sequestrate Anionic Dye**" in the partial fulfilment for the award of the degree of **Master of Science** in the **Department of Applied Chemistry, Delhi Technological University** is an authentic record of our own work carried out under the supervision of **Dr. ANIL KUMAR (Professor, Department of Applied Chemistry, Delhi Technological University)**.
We further declare that the dissertation has not been submitted by us for the award of any other degree of this or any other Institute.

HARSHITA THAPA
2K24/MSCCHE/31

JYOTI TOMAR
2K24/MSCCHE/51



DELHI TECHNOLOGICAL UNIVERSITY

(Formerly Delhi College of Engineering)
Shahbad Daulatpur, Main Bawana Road, Delhi-42

CERTIFICATE

This is to certify that the Project report entitled "**Biogenic Synthesis of NiO Nanoparticles using *Ficus Religiosa* and their application to Sequestrate Anionic Dye**" which is submitted by **Harshita Thapa (2K24/MSCCHE/31)** and **Jyoti Tomar (2K24/MSCCHE/51)**, Department of Applied Chemistry, Delhi Technological University, Delhi in partial fulfilment of the requirement for the award of the degree of **Master of Science**, is a record of the project work carried out by the students under my supervision. To the best of my knowledge, this work has not been submitted in part or full for any Degree or Diploma to this University or elsewhere.

Dr. Anil Kumar
(Supervisor)
Professor
Department of Applied Chemistry
Delhi Technological University
New Delhi – 110042

DELHI TECHNOLOGICAL UNIVERSITY
(Formerly Delhi College of Engineering)
Shahbad Daulatpur, Main Bawana Road, Delhi-42

PLAGIARISM VERIFICATION

Title of the thesis **"Biogenic Synthesis of NiO Nanoparticles using *Ficus Religiosa* and their application to Sequestrate Anionic Dye."**

This is to report that the above thesis was scanned for similarity detection. Process and outcome is given below:

Software used: Turnitin
Similarity Index: 10%
Total Word Count: 9140

Date: **16 June 2026**

HARSHITA THAPA
(2K24/MSCCHE/31)

JYOTI TOMAR
(2K24/MSCCHE/51)

Prof. ANIL KUMAR
(SUPERVISOR)

NOVELTY STATEMENT

In this study, waste leaves of *Ficus religiosa* (FR), commonly known as peepal an indigenous plant. The leaves were used as a green reducing and stabilizing agent for the synthesis of nickel oxide nanoparticles (NiO NPs). The synthesized NiO NPs were then applied for the removal of Congo Red (CR) dye from aqueous solution through batch adsorption experiments.

To the best of our knowledge, no previous study has reported the green synthesis of NiO NPs using *Ficus religiosa* waste leaves specifically for sequestration of CR. The FR-mediated NiO NPs exhibited good removal performance compared with conventionally synthesized control NiO NPs, mainly due to their higher surface area and improved water stability. These properties make the synthesized nanomaterial make efficient for anionic dye removal Therefore, this work presents a novel, eco-friendly, facile, and potentially scalable alternative to conventional and costly adsorbents. This approach introduces a novel, eco-friendly, green, facile and scalable alternative to conventional and more expensive adsorbents. It highlighting its potential for real-world wastewater treatment applications.

ABSTRACT

This study demonstrates the use of *Ficus Religiosa* (FR) leaves as a natural, cost-effective, green stabilizing and capping agent for the synthesis of Nickel Oxide (NiO) nanoparticles for the sequestration of anionic Congo Red (CR). Various techniques, including FTIR, XRD, FESEM, DLS, BET, HRTEM, and a UV-Vis spectrophotometer, were employed to demonstrate the efficiency of the synthesized NiO (FR) NPs as a biosorbent. The crystallite size of the nanoparticles was found to be 5 nm for NiO NPs (control) and 2.8 nm for Ni (FR) NPs calculated using XRD. The adsorption behaviour of the biosorbent was examined by varying several parameters, such as pH, dye concentration, adsorbent amount, and equilibrium time. Adsorption isotherms and kinetic models were also fitted. The maximum adsorption capacity of CR on biogenically synthesized NiO NPs was found to be 17 mg/g achieved at 37°C or 310.15 K. Isotherm and kinetic study revealed that Langmuir and Pseudo-First order was found to be best fit. The recyclability of the adsorbent remains good after 7 cycles of regeneration, with the adsorbent achieving ~83% removal using the real wastewater sample. Overall, NiO (FR) NPs, as a sorbent based on dried FR leaves, exhibit strong potential as an effective biosorbent for the adsorption of CR via contaminated water.

Keywords: Ficus Religiosa; Biomass; Biosorbent; Sequestration; Anionic Dye.

Graphical Abstract:

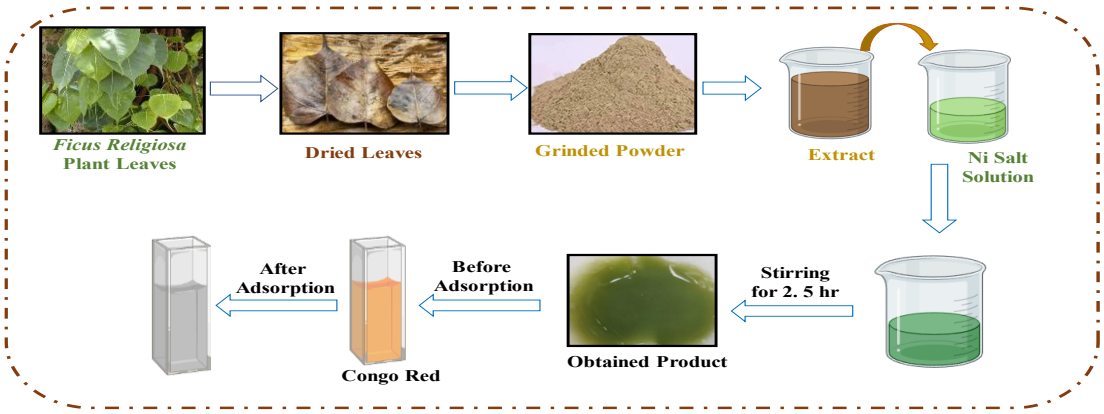


TABLE OF CONTENTS

TITLE	PAGE NO.
Acknowledgement	ii
Declaration	iii
Certificate	iv
Plagiarism verification	v
Novelty statement	vi
Abstract	vii
Contents	viii
List of Tables	x
List of Figures	xi

CHAPTER 1

INTRODUCTION……1

CHAPTER 2

MATERIALS AND METHODS……..5

2.1 Instrumentation

2. 2 Synthesis

2.2.1 Collection and extract preparation of *Ficus Religiosa* (FR)

2.2.2 Synthesis of NiO NPs by FR extract and without extract

CHAPTER 3

EXPERIMENTATION……..8

3.1 Batch analysis

3.2 Kinetics

3.3 Isotherms

CHAPTER 4

RESULTS AND DISCUSSIONS……11

4.1 Characterization

4.1.1 FTIR

4.1.2 XRD

4.1.3 FESEM

4.1.4 DLS

4.1.5 BET

4.1.6 Uv-Visible spectra

4.1.7 HRTEM

4.2 Adsorption studies

4.2.1 Equilibrium time

4.2.2 Dye concentration

4.2.3 Adsorbent dosage

4.2.4 pH

4.3 Probable Mechanism

4.4 Kinetics

4.5 Isotherms

4.6 Thermodynamics

4.7 Regeneration

4.8 Different water samples

4.9 Comparison with another adsorbent

CHAPTER 5

CONCLUSION…….38

REFERENCES……..39

LIST OF TABLES

Table 1: Calculated parameters using both models

Table 2: Calculated parameters using various models

Table 3: Temperature-dependent parameters for CR uptake

Table 4: Comparison of synthesized adsorbent with available literature

LIST OF FIGURES

Figure 1. Schematic representation of NiO (FR) NPs

Figure 2. Plots of (a) FTIR and (b) XRD of NiO NPs (control and NiO (FR) NPs.

Figure 3. Microscopic images of (a) NiO NPs (control) and (b) NiO (FR) NPs at 200 nm scale.

Figure 4. EDX mapping of NiO NPs (control)

Figure 5. EDX mapping of NiO (FR) NPs.

Figure 6. Zeta Potential plot of (a) NiO NPs (control) and (b) NiO (FR) Nps**.**

Figure 7. Plots of N_2 adsorption and desorption using BET (a) NiO NPs (control) and (b) NiO (FR) NPs.

Figure 8. UV-visible spectra of NiO (FR) NPs using UV-vis spectrophotometer ranges from 200-800 nm.

Figure 9. HRTEM images of (a) NiONPs (control); (b) NiO (FR) NPs at 20 nm, and (c) size distribution curve for NiO (FR) NPs.

Figure 10. (a) Plot of UV-Visible spectrophotometer and (b) Plot for equilibrium time at initial concentration 30 mg/L, adsorbent dosage 0.1 g, pH neutral, agitating speed 400 rpm.

Figure 11. Plots of (a) effect of dye concentration adsorbent dosage 0.1 g, pH neutral, agitating speed 400 rpm, and contact time 25 min, and (b) effect of adsorbent dosage at concentration 30 mg/L, pH neutral, agitating speed 400 rpm, and contact time 25 min.

Figure 12. (a) Plots of the effect of pH on dye removal at concentration 30 mg/L, adsorbent dosage 0.1 g, agitating speed 400 rpm, and contact time 25 min, and (b) Plausible mechanism of dye adsorption.

Figure 13. Plots of (a) First order and (b) Pseudo Second Order

Figure 14. Plot of linear models of (a) Langmuir and (b) Freundlich

Figure 15. Plot for (a) ln K versus 1/T for CR and (b) impact of temperature on adsorption capacity for CR.

Figure 16. Plot of (a) regeneration cycles of NiO (FR) NPs, and (b) dye removal efficiency from different water sample.

CHAPTER 1

INTRODUCTION

Currently, globally, industrial effluents, agricultural runoff, and municipal wastewater are the primary sources of water pollution, posing a significant threat to flora and fauna [1]. Freshwater systems are under tremendous strain due to increased industrialization, urbanization, agricultural intensification, and population growth, resulting in widespread water scarcity and declining water quality [2]. Currently, Industrial discharge into water bodies is one of the biggest risks to aquatic life and public health. Several hazardous materials are discharged into natural water bodies through scantily treated effluents, polluting the water [3].

Among all the pollutants, synthetic dyes are the most hazardous contaminants in industrial effluents, especially those used in the textile, leather, paper printing, cosmetic, plastic, rubber, pharmaceutical, and food processing sectors. Eliminating these dyes from wastewater poses a significant challenge due to their design, which ensures they remain chemically stable and resistant to factors like light, heat, and microbial decay [4,5]. A disturbed ecological balance and ecosystem result from the deterioration of the environment due to air, water, and soil pollution [6]. Dyes impart an intense color to water, even at low concentrations, which hinders the process of photosynthesis by decreasing light penetration and disturbing aquatic ecosystems. Furthermore, several synthetic dyes and their degradation byproducts exhibit toxic, mutagenic, and carcinogenic properties, posing a significant threat to both humans and aquatic life [7,8].

Congo Red (CR), a common anionic azo dye was chosen as a model dye in the present study. It is widely used in textile and related industries, biological staining, paper printing, rubber production, and textile dyeing, is highly persistent in water, and is

associated with considerable toxicological concern [7]. Compared with many dyes, it has high chemical stability and resistance to degradation, which are attributed to its structural azo (-N=N-) linkages and aromatic rings. These traits make CR a recalcitrant pollutant because they enable it to persist in aquatic environments for extended periods [9,10]. Due to the Production of aromatic amines, during degradation, exposure to Congo Red has been link to negative health effects like allergic reactions, gastrointestinal distress, respiratory issues, and possible carcinogenicity. It disrupts the ecological balance in aquatic systems by lowering dissolved oxygen levels in water and harming fish, algae, and microorganisms [11,12]. Metal-based adsorbents are attractive for CR removal because metal-based nanoparticles often exhibit favorable affinity toward anionic pollutants under acidic to neutral conditions, where electrostatic attraction between the adsorbent surface and the negatively charged sulfonate groups of CR dye can promote adsorption [13,14]. Therefore, CR can be considered a highly toxic pollutant in aqueous solution. Furthermore, *Ficus religiosa* leaves were selected as a green synthesis resource because they are indigenous, abundant and contain phytochemicals such as flavonoids, phenolics, and tannins, which can function as natural reducing and stabilizing agents, making the synthesis route more facile, sustainable, and eco-friendly [15].

Therefore, to overcome this issue, effective treatment methods are required for the wastewater treatment to eliminate the toxicity and persistence of Congo Red. Different methods, such as Membrane filtration, coagulation-flocculation, chemical oxidation, ozonation, ion exchange, precipitation, electrochemical treatment, and photodegradation, are amongst the conventional treatment techniques that have been developed over time [16–20]. Although these technologies can remove effluent, they often come with disadvantages, such as high operational costs, complicated infrastructure demands, excessive energy consumption, secondary sludge generation, and limited effectiveness against stable azo dyes. Thus, an alternate method of dye remediation is adsorption, which is effective, and ecologically sustainable, easy to use, affordable, highly efficient, and able to adapt to various pollutants. The success of adsorption significantly depends on the type of adsorbent material, its surface characteristics, porosity, and functional groups [21].

Numerous adsorbents have been explored and investigated, including activated carbon, clays, polymers, nanomaterials, and materials derived from biomass [22–25]. Among these, nanomaterials have garnered significant interest due to their remarkable surface area, enhanced reactivity, and adjustable surface chemistry [26–28]. Metal nanoparticles, in particular, have shown exceptional potential in environmental remediation due to their high adsorption capacity, catalytic activity, and ability to degrade organic pollutants [29–32]. Beigi and the group has used pyrolized NiO based metal organic framework for for enhanced removal capacity [33]. Mohamed and group have synthesized seaweed biomass based composite for the removal of azo dyes [34]. Wandu and the group have synthesized NiO NPs *Calpurnia Aurea* leaf extract and used for sequestration of malechite green dye [35]. Since nickel oxide (NiO) is reasonably abundant, affordable, and has superior catalytic, magnetic, and redox properties, nickel Oxide nanoparticles (NiO NPs) are particularly interesting. NiO NPs have proven effective in wastewater treatment, heavy metal removal, antimicrobial coatings, and dye degradation [12,36,37].

However, traditional physical and chemical synthesis methods for NiO NPs have often involved the use of hazardous solvents, toxic reducing agents, and high energy inputs, which limit their sustainable use and raise concerns about health and the environment. Therefore, the green method for synthesizing nanoparticles using biological resources has become widely acknowledged as an environmentally friendly solution to these problems. By using renewable biological materials, consuming low energy, and minimizing the use of hazardous chemicals. Plant-mediated nanoparticles synthesis has become the most viable and scalable biological synthesis technique [38]. Because plant extracts contain a variety of phytochemicals, including flavonoids, phenolics, tannins, terpenoids, sugars, and proteins, they simultaneously function as reducing, capping, and stabilizing agents [39,40].

The *Ficus religiosa L.,* commonly known as ‘Peepal’*, is a* member of the Moraceae family and is found all over the Indian sub-continent. Many plant parts of the peepal tree are traditionally used to treat respiratory conditions, diabetes, infections and

inflammatory disorders [41]. The peepal trees are both culturally and medicinally significant. According to phytochemical analysis, peepal leaves contain Flavonoids, Phenolic acid, Tannins, Saponins, and Terpenoids, which possess strong anti-oxidant & reducing properties [42].

In recent studies, *Ficus religiosa* leaf extract has been shown to biosynthesize silver and gold nanoparticles, demonstrating its reducing potential capability and capacity to stabilize nanoparticles [43], [44]. However, despite these developments, there is still much to learn about the environmentally friendly synthesis of NiO NPs using peepal leaf extract.

There are further environmental advantages to using peepal leaf biomass for the synthesis of nanoparticles. Every year, Peepal trees produce a significant amount of leaf litter, most of which is still unutilized. The process of turning the low-value biomass into useful nanoparticles promotes sustainable resource management and waste utilization [45]. Despite the growing interest in green nanotechnology, there is a substantial research gap in the synthesis of NiO NPs from indigenous plant resources and their use in Congo Red dye remediation. There are currently few systematic studies looking at adsorption performance, nanoparticle properties, and synthesis parameters. Thus, the goal of this research is to develop an efficient, cost-effective, and eco-friendly method for wastewater sequestration, utilizing NiO NPs synthesized through a green method. Thus, to achieve the main aim, the leaf extract of Peepal was used as a stabilizing and capping agent for the synthesis of NiO NPs in a sustainable and environmentally friendly manner. The synthesized NPs are used to remove the Congo Red dye from aqueous solutions. Furthermore, to examine the important factors, such as temperature, initial dye concentration, adsorbent dosage, pH, and contact time, that affect the adsorption efficiency, an experiment was performed.

CHAPTER 2

MATERIALS AND METHODS

The primary raw material for the experiments was leaves of the Ficus religiosa tree (peepal), collected from a local area of Rewari, Haryana, India, located at 28.1920° N latitude and 76.7191° E longitude. The reference dye used was Congo red, purchased from Thermo Fisher Scientific (India). Sodium hydroxide (NaOH, 97%), ethanol (99%), and acetone (99%), supplied by Sisco Research Laboratories (Delhi). Concentrated hydrochloric acid (35-38%) purchased from the Central Drug House (India). All the experiments were conducted using distilled water.

2.1 Instrumentations

FTIR spectra were performed on a PerkinElmer FTIR spectrometer in the range of 400-4000 cm^{-1} to identify the functional groups. Crystal structure was determined using PXRD with a Bruker D8 Advance diffractometer. An X-ray diffractometer was used to assess the crystallinity of the synthesized material, with the Bruker D8 Advance operating at Cu Kα radiation (λ = 1.5418 Å) over a 2θ range of 10-100°. Field-emission scanning electron microscopy (FESEM) on a JEOL JSM-6610LV instrument was used to analyze the surface morphology of the material. The specific surface area and pore size distribution, were determined using Brunauer–Emmett–Teller (BET) analyses with a Quanta Chrome Nova Win device at 77 K. Surface charge behaviour was evaluated through zeta potential measurements conducted via dynamic light scattering (DLS) using a Malvern Zeta-sizer Nano ZSP. A Shimadzu UV-Vis 1900i spectrophotometer (Japan), used to measure dye concentrations at room temperature, with a maximum wavelength (λ_{max}) of 498 nm. A calibrated pH meter from Eutech

Scientific was used to measure and adjust the pH of the solution. To ensure reproducibility, each experiment was performed in triplicate.

2. 2 Synthesis

2.2.1 Collection and extract preparation of *Ficus Religiosa* (FR)

Initially, FR leaves were collected from nearby areas of Rewari in November 2025. The leaves were first cleaned with normal water, then by distilled water (DW) to eliminate dirt and debris. Then, the leaves were sun-dried for one day to remove the water content, followed by oven drying at 50 °C. The dried leaves were then crushed into powder using a regular domestic mixer grinder. The obtained crushed powder of leaves was then sieved to obtain a fine, homogeneous particle powder and stored in an airtight container, which was later subjected to prepare an extract.

For the extraction of FR, 1 g of FR was dissolved in 100 mL of DW and stirred for 3 hours at 100 °C. Then, the obtained solution was filtered, and the extract was stored in a freezer.

2.2.2 Synthesis of NiO NPs by FR extract and without extract

100 ml solution of 0.1M Ni $(NO_3)_2$. $6H_2O$ salt was prepared in distilled water. The solution was divided into equal halves (50 mL each). In one beaker containing 50 mL of salt solution, the solution was stirred continuously. Then, 20 mL of leaf extract was dropwise added into the solution, and a colour change from green to dark green was observed. Similarly, in another beaker, the leaf extract is not added. Then, place both beakers on a stirrer at room temperature, and stirring was maintained at 400 rpm for 30 minutes. Furthermore, the pH of the solution was recorded and adjusted to pH 10 for both solutions by dropwise addition of 1 M NaOH solution, resulting in turbidity in the solution. Then, place the beakers on the stirrer for 2 hours. At last, filter both the

solutions, washed with ethanol followed by water, and dried. The dried powder was then calcined at 350 °C for 3 hours in a muffle furnace, as shown in Figure 1. The obtained product was ground, characterized, and utilized to sequestrate anionic CR dye from the aqueous medium.

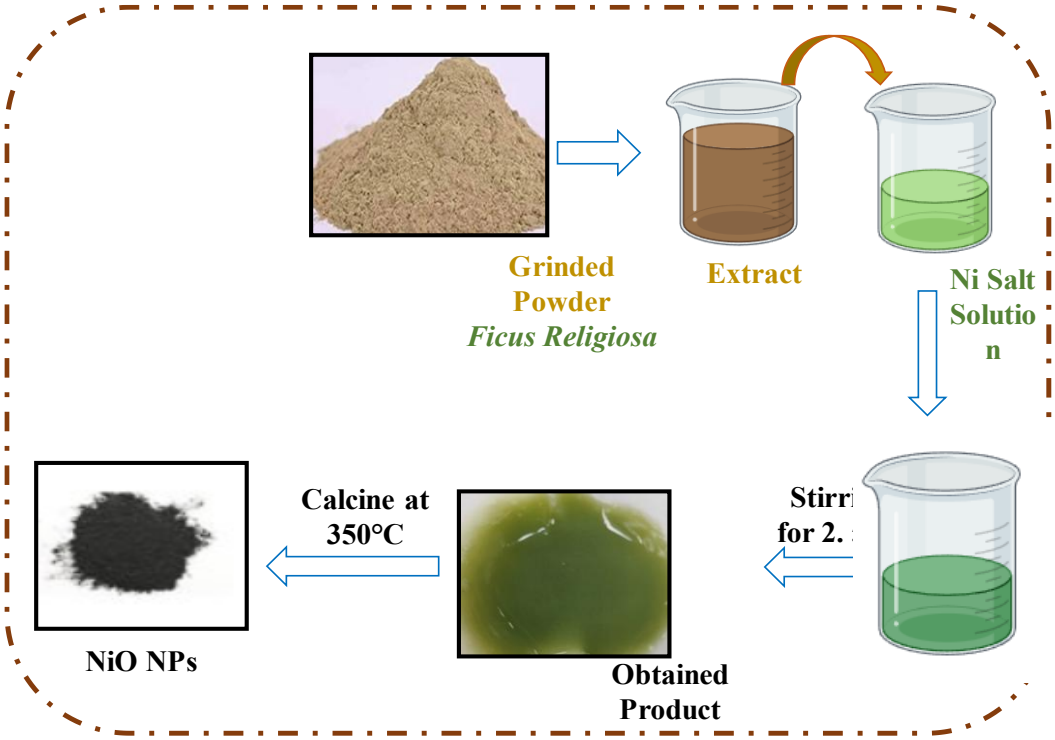


Figure 1. Schematic representation of NiO (FR) NPs

CHAPTER 3

EXPERIMENTATION

3.1 Batch analysis

To evaluate the adsorption efficiency of the synthesized nanoparticles as a sorbent, batch adsorption experiments were conducted, focusing on the effect of contact time. 0.1 g of adsorbent in 100 mL of Congo red dye solution. This solution was placed on a magnetic stirrer to ensure proper interaction between the adsorbent and the dye molecules. The stirring was continued for approximately 30 min at room temperature. To check the progress of % dye adsorption, aliquots were withdrawn at regular intervals. At each interval, 3 mL of the solution was withdrawn into test tubes from the reaction mixture. The absorbance was recorded using a UV-vis spectrophotometer at 497 nm. Further, the percentage of dye removal (% DR) and adsorption capacity at equilibrium (q_e) were calculated using equations (1) and (2) [46]:

$$\%\,\mathrm{DR} = \frac{C_0 - C_t}{C_0} \times 100 \qquad (1)$$

$$q_e = (C_0 - C_t) \times \left(\frac{V}{W}\right) \qquad (2)$$

Here, C_0 is the dye concentration (blank), and C_t is the concentration at time *t, V* is the volume of solution, and W is the weight of adsorbent.

3.2 Kinetics

The first-order model accounts for physical adsorption and predicts that the changes in adsorbate removal rate and concentration with time. The linear expression as [47].

$$ln(q_e - q_t) = lnq_e - K_1 t \quad (3)$$

Here, q_e and q_t are the adsorbent uptake capacity (mg g^{-1}) of dye at equilibrium and at time 't'. K_1 is the rate constant (min^{-1}).

The adsorption kinetics rate equation for pseudo-second order is expressed in linear form as [48]:

$$\frac{t}{q_t} = \frac{1}{k_2 q_e^2} + \frac{t}{q_e} \quad (4)$$

Here, q_t (mg g^{-1}) represents the dye uptake of the adsorbent at time t. The rate constant is determined by k_2 (min^{-1}).

The initial adsorption rate 'h' (mg g^{-1} min^{-1}) can be determined by the equation

$$h = k_2 q_e^2 \quad (5)$$

3.3 Isotherms

It is feasible to demonstrate the different kinds of interactions between the adsorbent and pollutants in terms of the adsorbent surface features by incorporating the obtained adsorption data into models, such as the Langmuir and the Freundlich models.

The Langmuir isotherm model predicts that adsorption occurs in a monolayer on the homogeneous surface of an adsorbent. Additionally, it suggests that molecules

adsorbed onto adjacent sites do not interact with one another, and that the sorbent's surface contains only a limited number of active sites. The equation used is expressed as [49].

$$\frac{c_e}{q_e} = \frac{1}{\mathrm{k_L} q_{\max}} + \frac{c_e}{q_{max}} \qquad (6)$$

q_{max} (mg g^{-1}) presented the maximum uptake capabilities of CR, and q_e (mg g^{-1}) represents the saturation adsorption capacities. While C_e (mg L^{-1}) represents equilibrium concentrations of CR, and K_L (L mg^{-1}) is the Langmuir constant.

The R_L is a unitless constant that determines linearity (R_L=1), irreversibility (R_L=0), favourability (0 < R_L <1), or un-favourability (R_L > 1) of adsorption and is calculated with the given formula.

$$\mathrm{R_L} = \frac{1}{1+\mathrm{k_L C_i}} \qquad (7)$$

Where CR solution concentration (mg L^{-1}) is given by C_i.

Freundlich isotherm, where adsorbate uptake occurs when heterogeneous binding sites are arranged in multilayers on sorbent surfaces at low concentrations. The logarithmic linear can be expressed as [50].

$$\log q_\mathrm{e} = \log \mathrm{K_f} + \frac{1}{n_\mathrm{f}} \log C_e \qquad (8)$$

Here, q_e refers to adsorption capacities (mg g^{-1}), C_e representing the equilibrium concentration of CR dye (mg L^{-1}). While Freundlich coefficients, K_f [(mg g^{-1}) (L mg^{-1}) $1/n_f$], represent the uptake capacity of adsorbate, and n_f indicates the heterogeneous adsorption intensity.

CHAPTER 4

RESULTS AND DISCUSSIONS

4.1 Characterization

4.1.1 FTIR

The FTIR spectra of NiO NPs (Control) and NiO (FR) NPs are shown in Figure 2a, providing information on the functional groups present in the materials. In NiO(FR) NPs the broadband at 3347 cm^{-1} is attributed to the OH band, while the relatively lesser broadening of this peak was observed at 3381 cm^{-1} [51–53]. The bands at 1637 cm^{-1},1351cm^{-1}, 974 cm^{-1}, in NiO NPs (control) and 1573 cm^{-1}, 1324 cm^{-1}, 1097 cm^{-1} confirm the presence of C=O, C=C, -C-H groups in the matrix [54,55]. While in the case of NiO (FR) NPs, a distinctive peak was observed at 531 cm^{-1} may be attributed to the Metal oxygen bond in the biogenically synthesized material [8]. However, peak is not visible in case of control hydrogel at lower region. It may be concluded, the absence of a clear Ni–O peak in the control FTIR spectrum should not be taken as evidence that NiO NPs was not formed, because FTIR is less definitive than XRD for confirming the oxide phase in such systems. There may be chance of weak vibration or overlapped of Ni–O in the control sample.

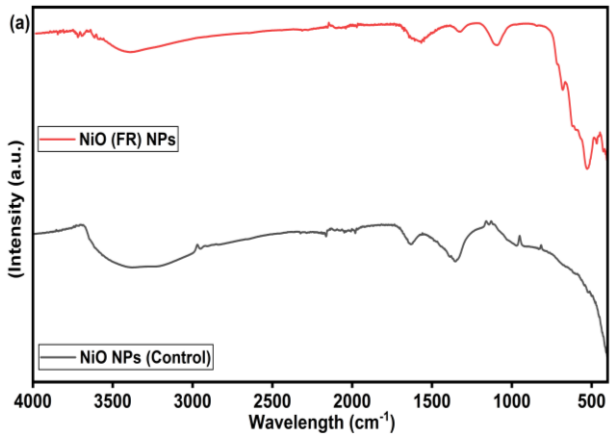
4.1.2 XRD

Figure 2b presents the PXRD pattern of NiO NPs (control) and NiO (FR) NPs. Both the NPs pattern shows a sharp and intense peak, while a more pronounced peak with sharper and more intense intensity was observed in bio-genically synthesized NPs as

compared to control NPs, which demonstrates that the synthesized NiO (FR) NPs have a more crystalline and pure nature of NiO NPs [56]. The XRD peaks observed for (NiO NPs (control) at 36.51°, 42.68°, 62.22°, 74.72°, 78.84°, and for NiO (FR) NPs at 36.86°, 43.04°, 62.54°, 75.07°, 79.08°, corresponding to (111), (200), (220), (311), and (222) planes, respectively, matched with JCPDS No 47-1049 [57]. The crystallite size was calculated using Debye Debye-Scherrer equation,

$$d = \frac{0.89\,\lambda}{\beta cos\theta} \qquad (10)$$

Here, X-ray wavelength is presented by λ, full width half maxima is β, and Bragg's diffraction angle is θ. The crystallite size was found to be 5 nm for NiO NPs (control) and 2.8 nm for Ni (FR) NPs. The d spacing was calculated and was found to be 0.244 Å for NiO NPs (control) and 0.201Å for Ni (FR) NPs.



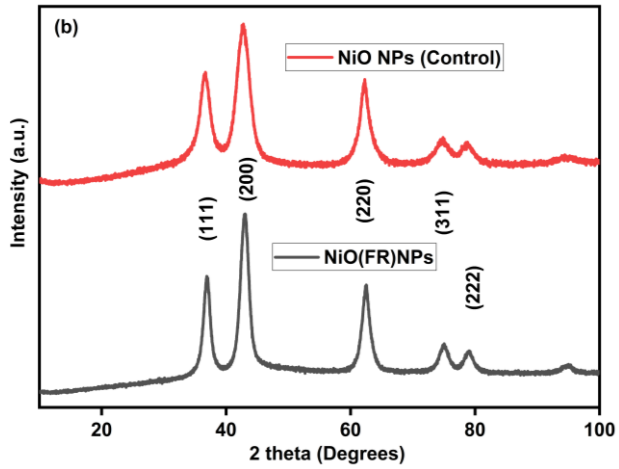


Figure 2. Plots of (a) FTIR and (b) XRD of NiO NPs (control and NiO (FR) NPs.

4.1.3 FESEM

In Figure 3, the NiO NPs (control) and NiO(FR) NPs microscopic images are shown. The fragmented morphology has been observed in similar size in NiO(FR) NPs, which may indicate more adsorption sites and significantly greater adsorption. While NiO Nps (control) exhibit a highly agglomerated, rough surface morphology composed of irregular sizes [56].

While in Figure 4 & 5, EDX mapping of the synthesized material is presented. It shows the presence of homogeneously dispersed Ni in the matrix.

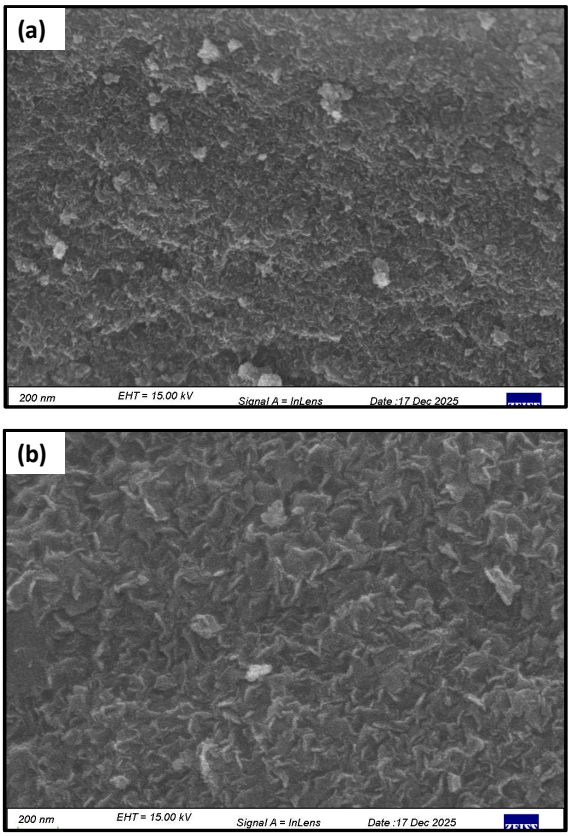


Figure 3. Microscopic images of (a) NiO NPs (control) and (b) NiO (FR) NPs at 200 nm scale.

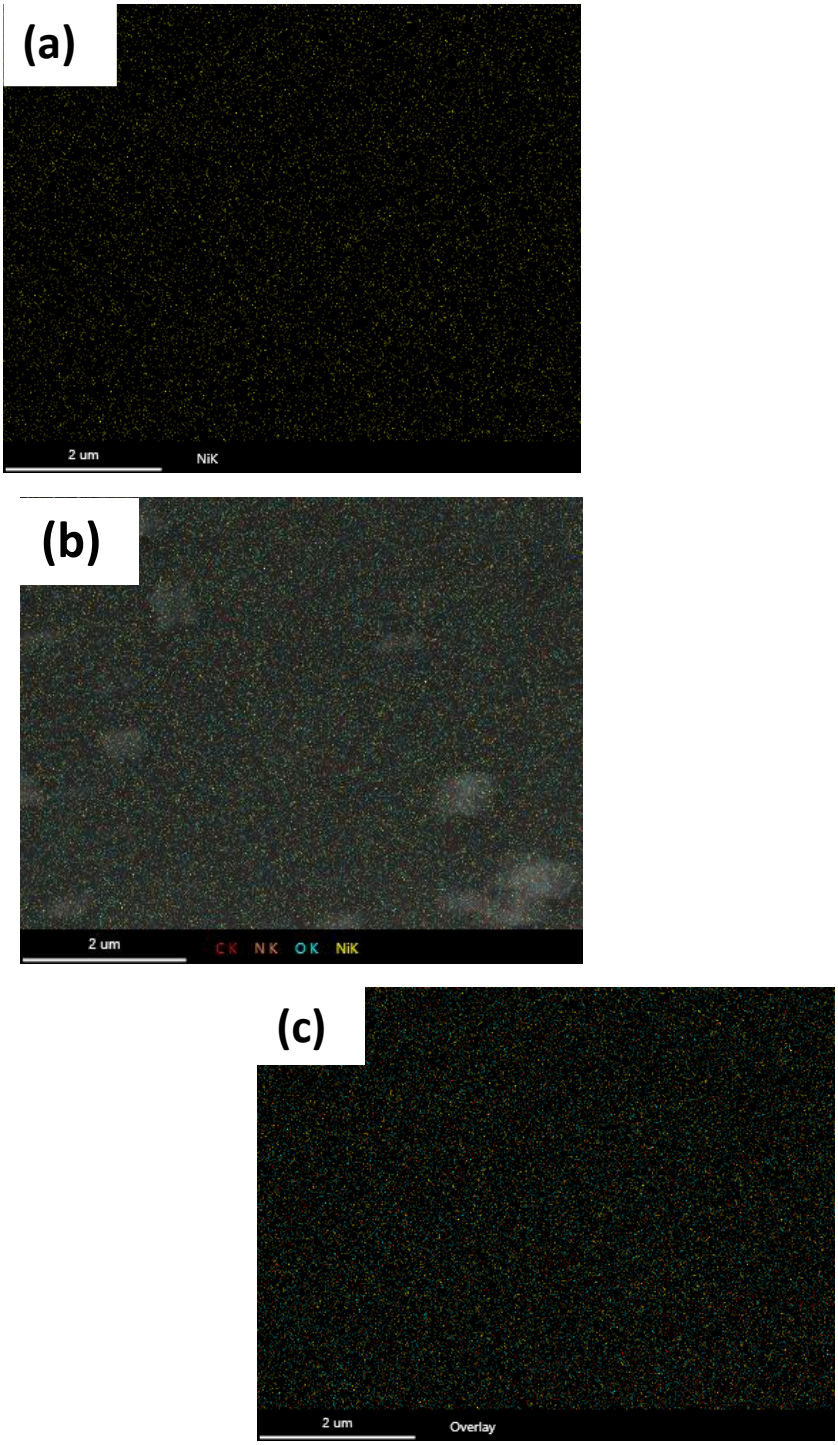


Figure 4. EDX mapping of NiO NPs (control)

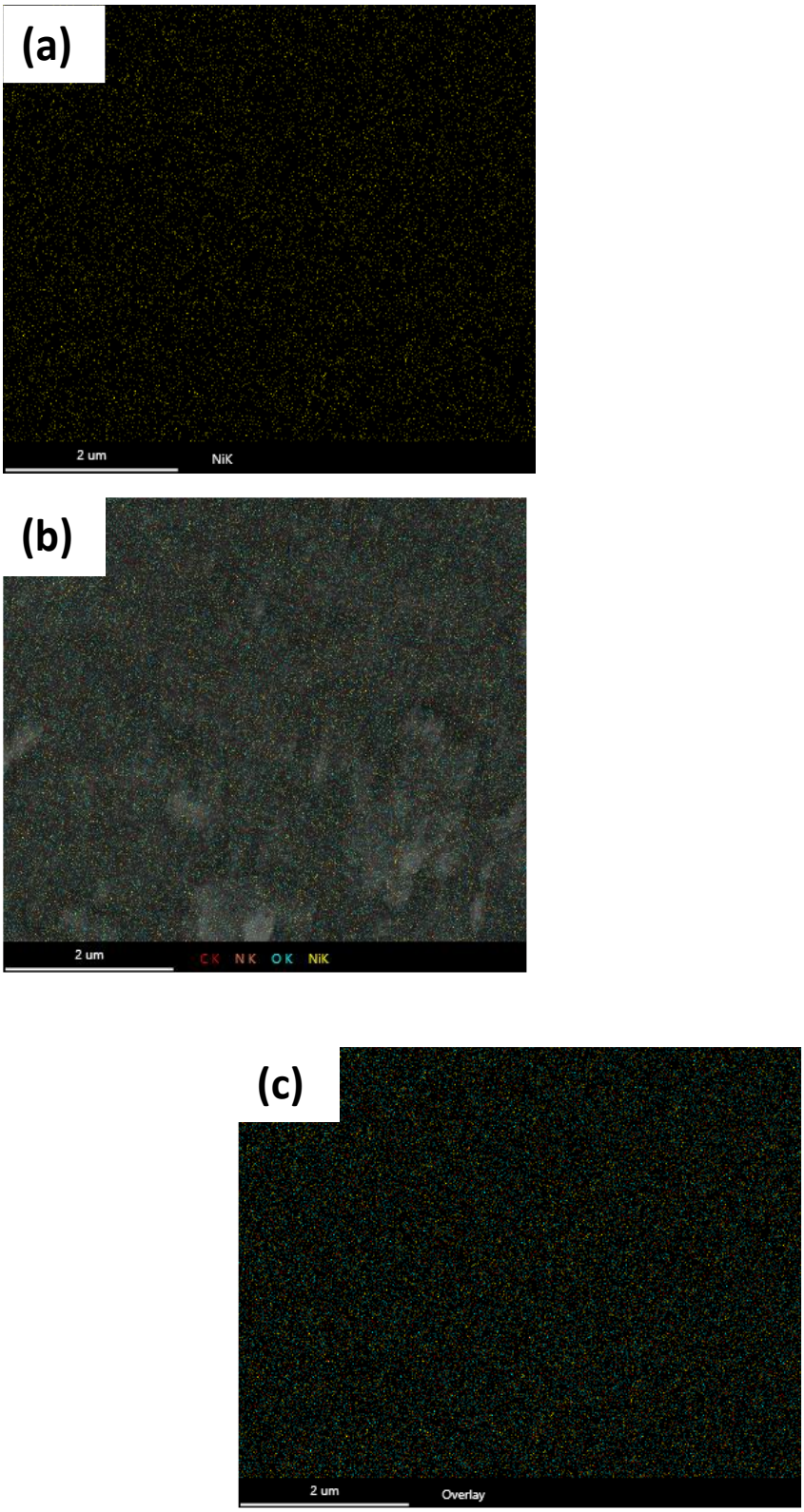
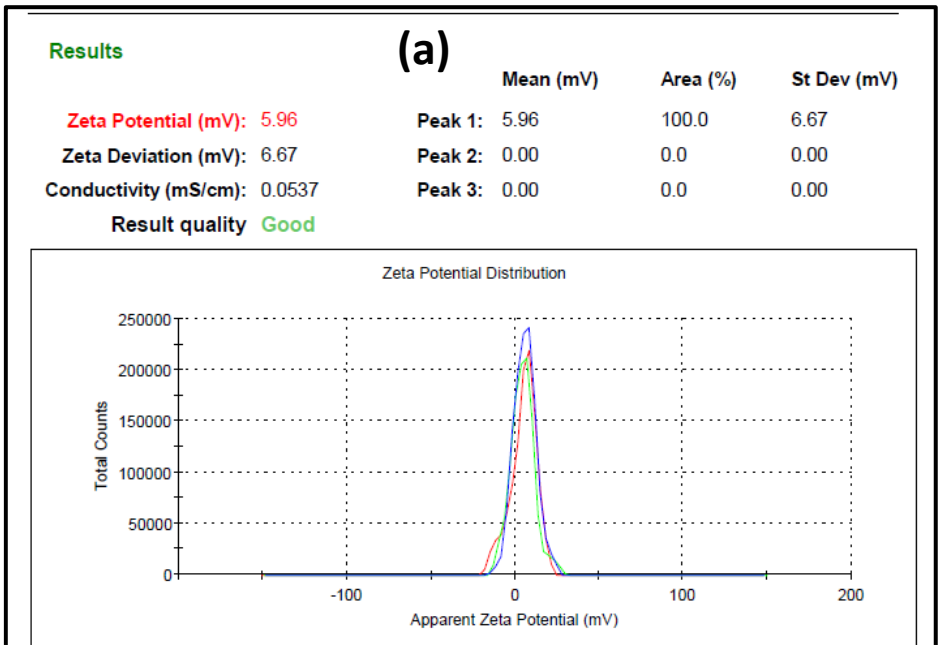


Figure 5. EDX mapping of NiO (FR) NPs.

4.1.4 DLS

The dynamic light scattering method is used to determine the zeta potential of the biosorbent. It will provide information about the stability and the charge of the biosorbent by measuring its zeta potential. It was found that NiO NPs (control) had a positive potential presented in Figure 6. While NiO(FR) NPs had a higher positive surface charge, which may show better synergistic interaction with the dye molecules, resulting in more pronounced dye adsorption over biosorbent surfaces using NiO(FR) NPs [19].



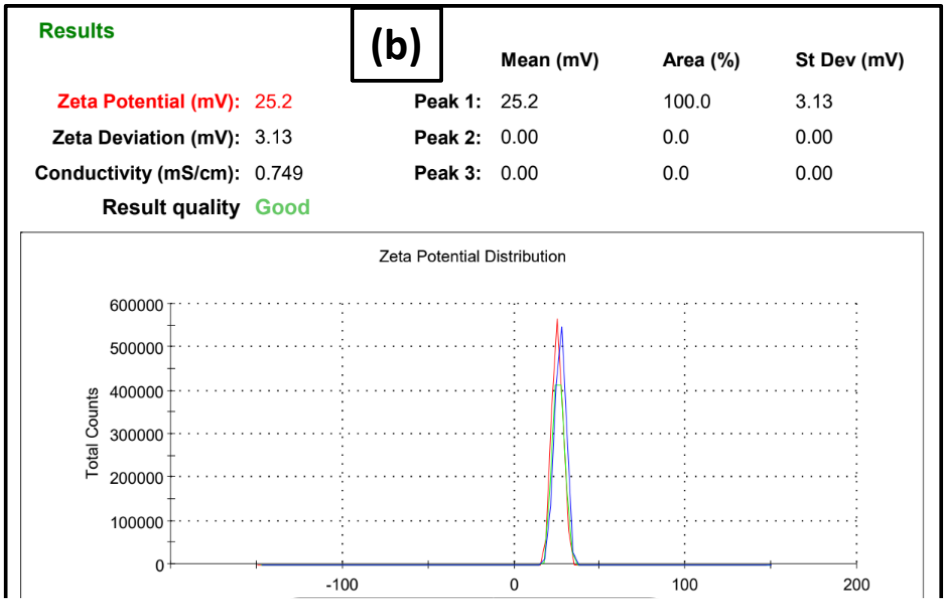


Figure 6. Zeta Potential plot of (a) NiO NPs (control) and (b) NiO (FR) Nps**.**

4.1.5 BET

The active surface area of NiO NPs (Control) and NiO (FR) NPs was estimated using Brunauer-Emmett-Teller (BET) analysis, as presented in Figure 7. It was found that the active surface areas were 33.902 m^2/g and 44.721 m^2/g, for NiO NPs (Control) and NiO (FR) NPs respectively. The pore diameters were found to be 17.535 Å and 19.388 Å, respectively. Hence, it was concluded that biogenically synthesized NiO (FR) NPs have a higher active surface area than control NiO NPS. It may be correlated with the higher dye removal efficiency of the effluent using NiO (FR) NPs.

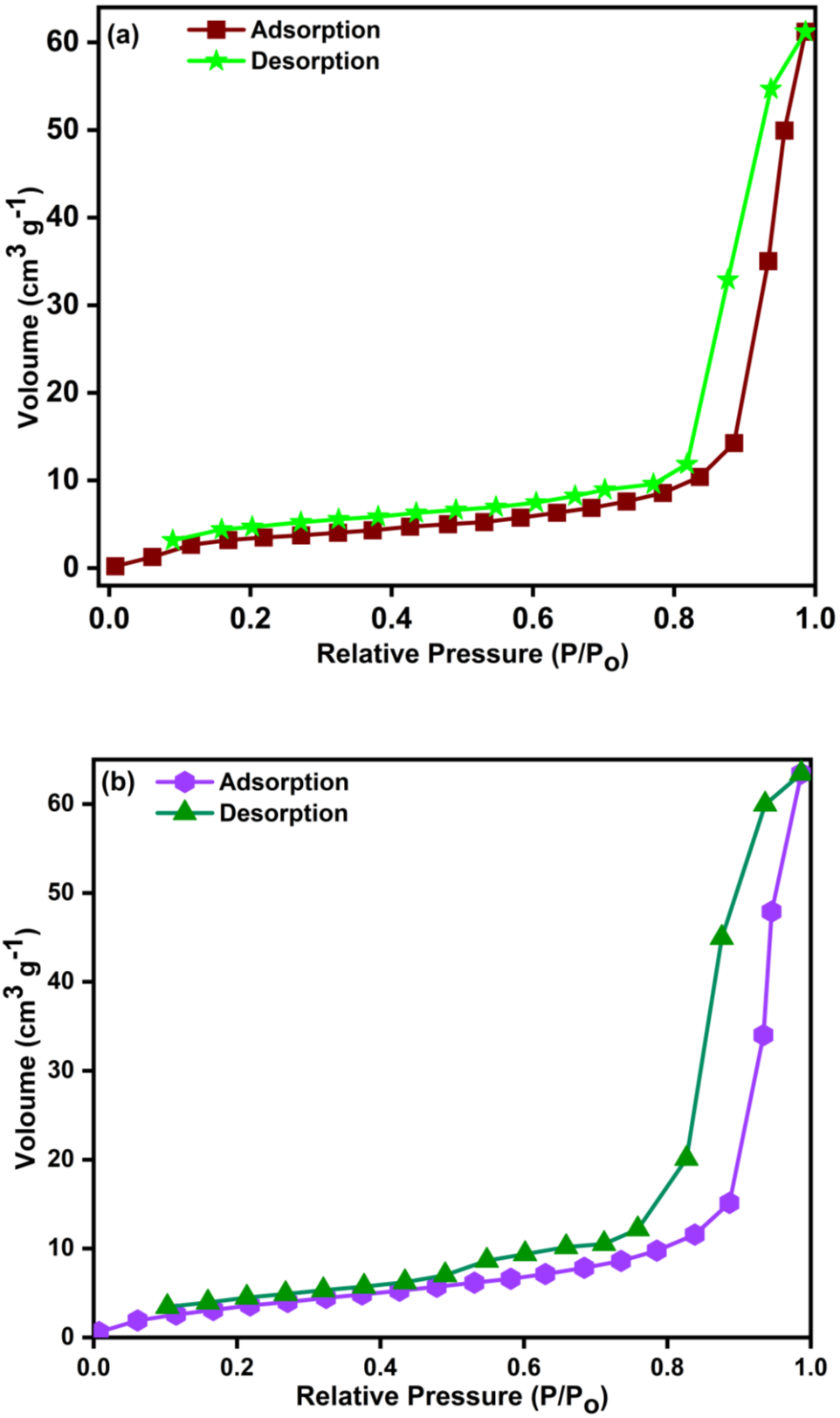


Figure 7. Plots of N_2 adsorption and desorption using BET (a) NiO NPs (control) and (b) NiO (FR) NPs.

4.1.6 UV- visible spectra

The UV-visible absorption spectra of NiO(FR) NPs are presented in Figure 8. The optical absorption peak was found to be at 269 nm. The band gap of the NiO(FR) NPs was calculated to be 5.3 eV. Kumar and the group has reported the similar band gap for the NiO NPs synthesized using green method [58].

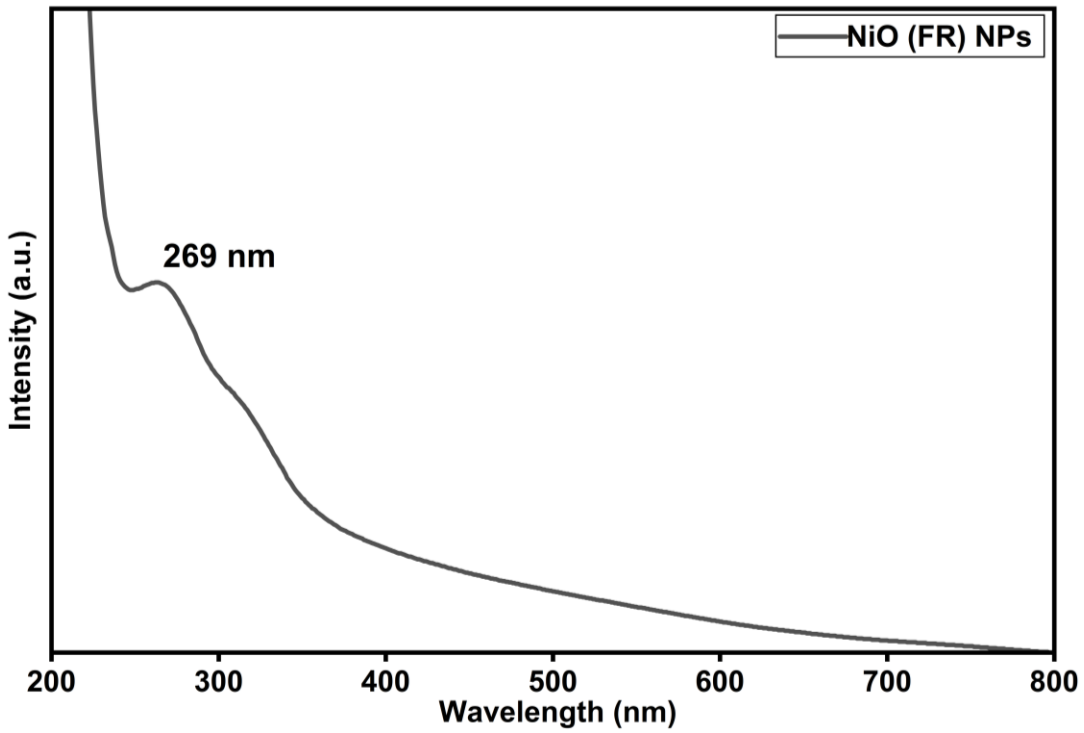


Figure 8. UV-visible spectra of NiO (FR) NPs using UV-vis spectrophotometer ranges from 200-800 nm.

4.1.7 HRTEM

Figure 9 shows the HRTEM images of the synthesized nanoparticles. It was observed that aggregated irregular shaped particles in the case of NiO (FR) NPs, and the average size was found to be 3.9 nm, which is in good agreement with the size calculated by Scherer's equation. While the size calculated for control NiO NPs was 4.7 nm, which was almost identical to that calculated from XRD peaks, the particles obtained were irregularly shaped [58,59].

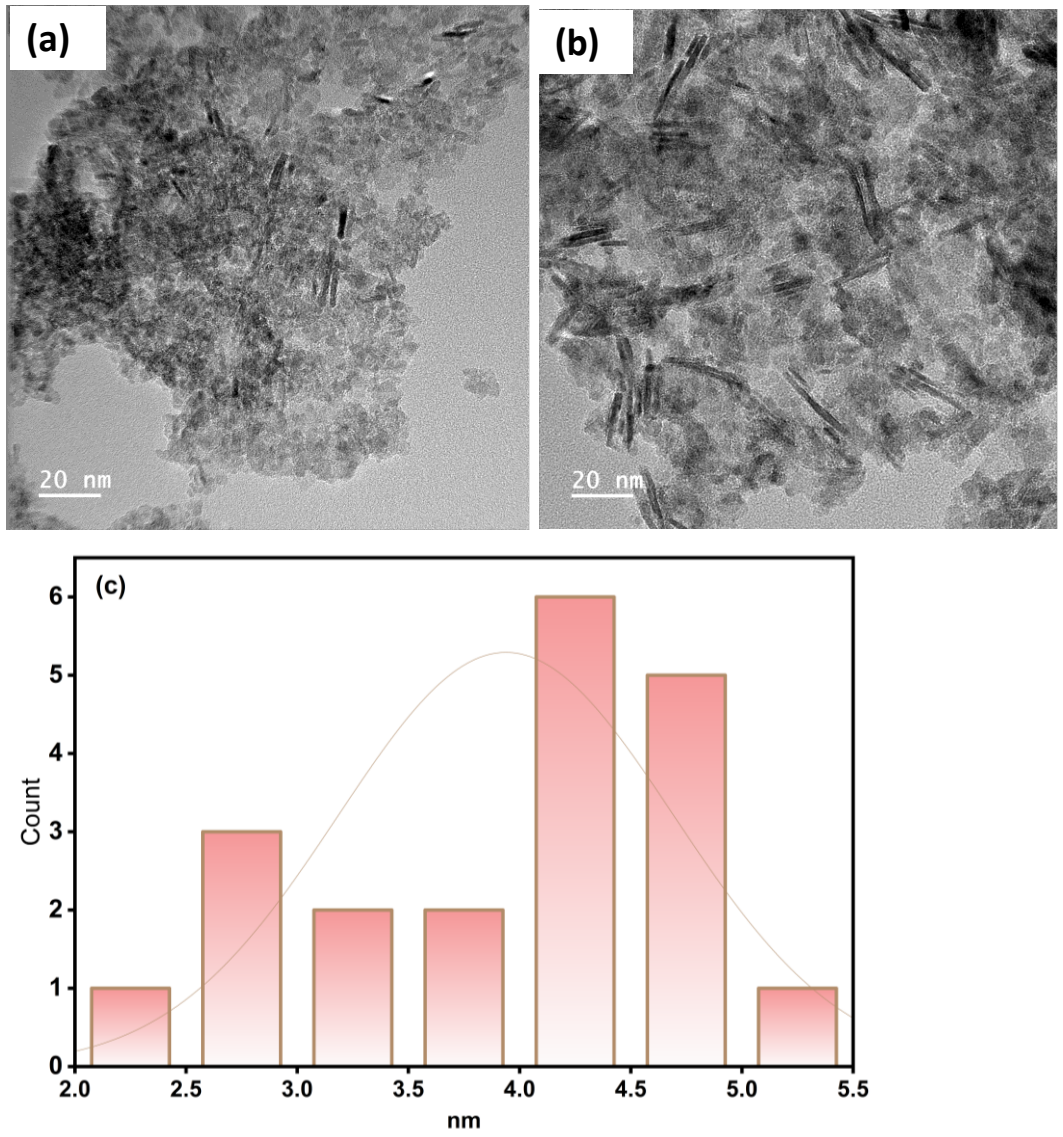


Figure 9. HRTEM images of (a) NiONPs (control); (b) NiO (FR) NPs at 20 nm, and (c) size distribution curve for NiO (FR) NPs.

4.2 Adsorption Studies

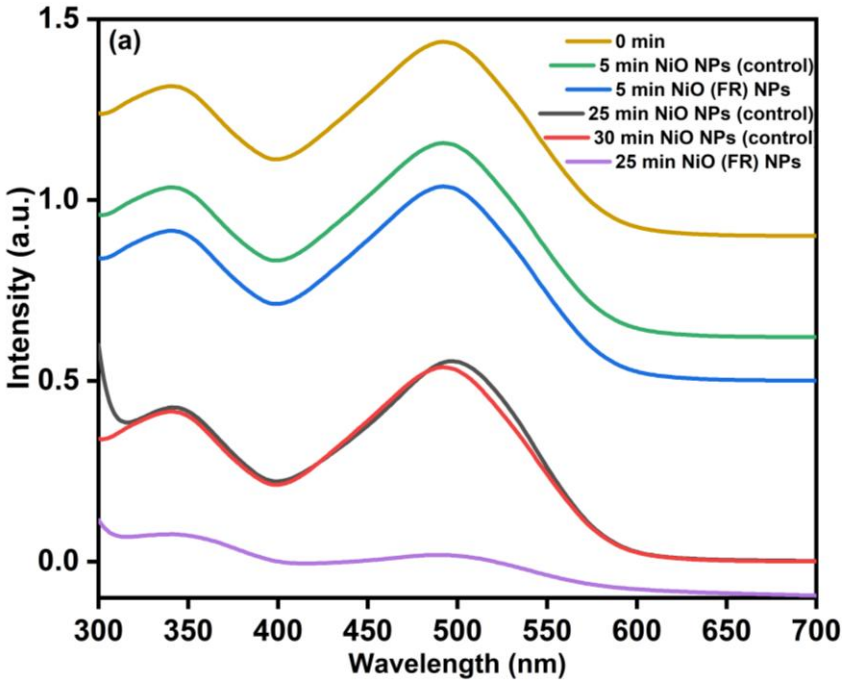
4.2.1 Equilibrium Time

The time between an adsorbent and a dye solution gives information about the reaction's equilibrium. Figure 10 shows the percentage of dye adsorption of the CR dye using FR utilized NiO NPs. It was observed that the percentage of dye adsorption increased from 88.63% after 10 minutes to 96.36% in 25 minutes. After 25 minutes, there was no noticeable change in the dye removal, indicating that the adsorbent's equilibrium had been reached [19]. This can be explained by the fact that the adsorption sites were initially available, resulting in higher adsorption. Later, as sites became occupied, equilibrium was reached in the process. Hence, the optimized contact time was set at 25 minutes for all experiments.

Similarly, the experiment was conducted for NiO NPs (control), and it was found that the dye removal was 63%. Therefore, further studies were conducted for extract extract-utilized NiO (FR) NPs.

It may be attributed to the fact that the advantageous surface and structural characteristics produced during green synthesis may be responsible for the enhanced CR removal effectiveness of the FR-mediated NiO NPs. Phytochemicals generated from plants can affect nucleation and growth by serving as reducing and capping agents. This often results in nanoparticles with larger specific surface area, smaller crystallite size, and an abundance of surface functional groups. The quantity of available active sites for adsorption is increased by the characteristics features of FR. Furthermore, the NiO NPs surface becomes positively charged when the pH falls below the zero charge threshold, which increases electrostatic attraction to the negatively charged sulfonate groups of Congo Red. The adsorption process may be further aided by π-related interactions and hydrogen bonding. Therefore, it can be

concluded that dye removal efficiency was enhanced in FR based NiO NPs as compare to control NPs.



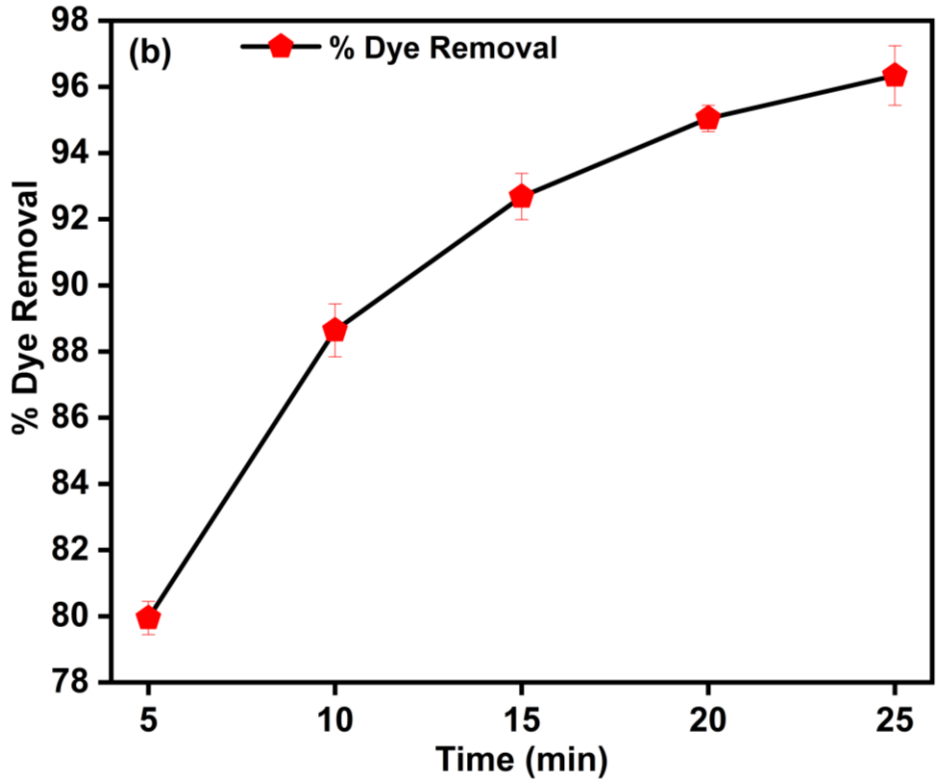


Figure 10. (a) Plot of UV-Visible spectrophotometer and (b) Plot for equilibrium time at initial concentration 30 mg/L, adsorbent dosage 0.1 g, pH neutral, agitating speed 400 rpm.

4.2.2 Dye concentration

Figure 11a illustrates the effect of dye concentration, ranging from 20 ppm to 70 ppm. The effect of dye concentration on adsorption was investigated, and it was found that as the dye concentration increased from 20 ppm to 70 ppm, the percentage of dye adsorption decreased from 96.36% to 43.19%. This can be attributed to the fact that at lower dye concentrations, there are fewer dye molecules, which can easily adsorb onto the synthetic adsorbent [60]. In contrast, at higher dye concentrations, an excessive number of CR molecules are present in the solution, resulting in saturation of the active sites [61,62].

4.2.3 Adsorbent Dosage

The aim of the dose study was to optimize the amount of adsorbent used in the adsorption study by immersing 0.05-0.2g of adsorbent in 30 ppm of CR dye, as shown in Figure 11b. It was found that the percentage of dye adsorption increased from 84.25% to 97.29% as the adsorbent dose rose from 0.05g to 0.2g. This can be explained as follows: a more adsorbent material has a larger surface area, which means there are more active sites available to adsorb the dye onto the adsorbent surface [63]. The dye adsorption was found to be almost similar (96.36%) after a further increase in dosage to 0.15g. It may suggest that the adsorbent becomes saturated with further increases, as a higher number of adsorbent molecules interact with each other, creating a hindrance that restricts the adsorption of dye molecules on the surface, resulting in no increase in adsorption beyond this point [64].

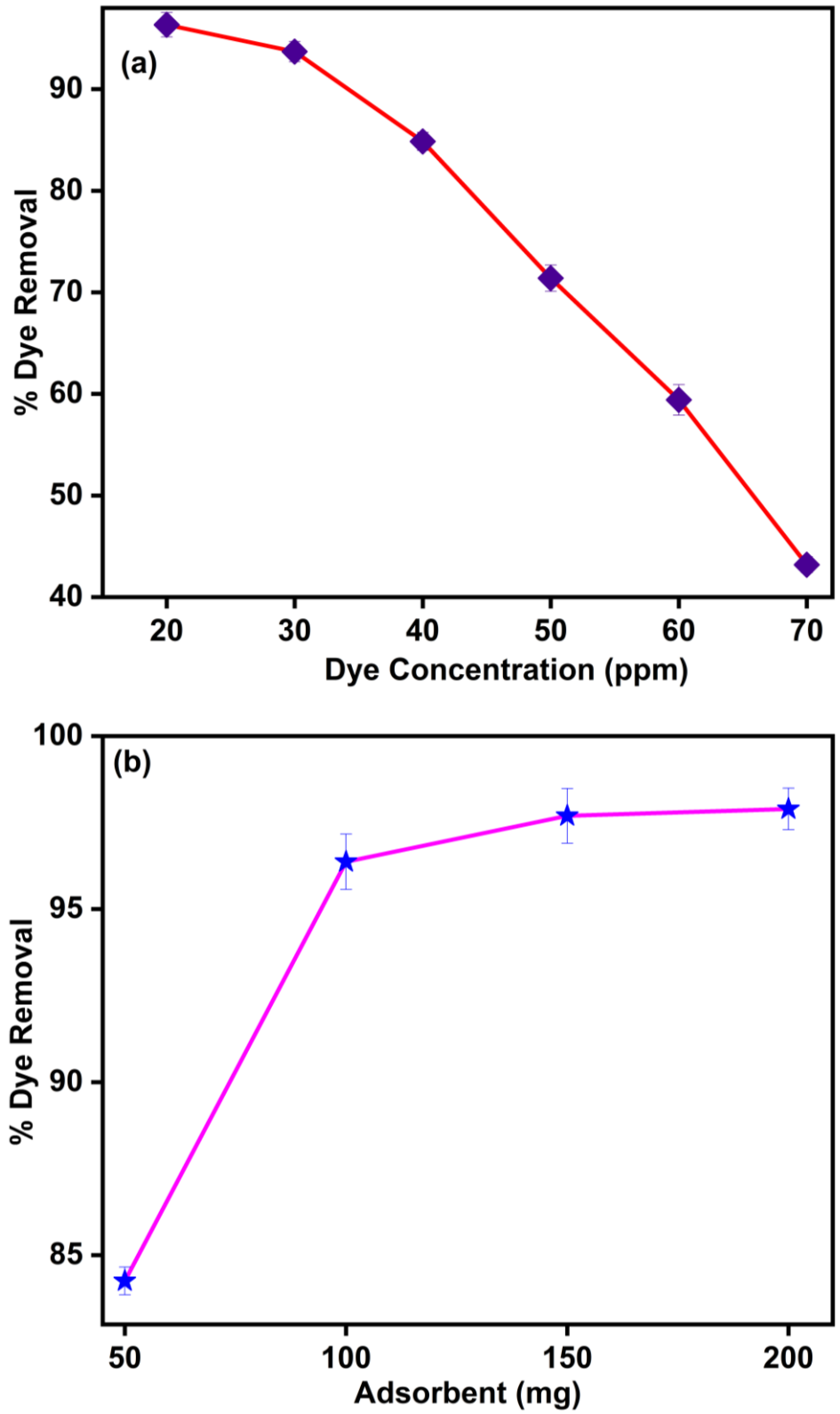


Figure 11. Plots of (a) effect of dye concentration adsorbent dosage 0.1 g, pH neutral, agitating speed 400 rpm, and contact time 25 min, and (b) effect of adsorbent dosage

at concentration 30 mg/L, pH neutral, agitating speed 400 rpm, and contact time 25 min.

4.2.4 pH

Figure 12a illustrates the effect of pH on CR adsorption by biogenically synthesized NiO (FR) NPs, as observed in the pH range of 5 to 9 using 0.1g of adsorbent and a reaction duration of 25 minutes. It was shown that when the pH rose from 5 to 9, the percentage of dye adsorption first increased up to pH 7, rising from 85.15% to 96.36%. The percentage of dye adsorption was found to decrease (96.36 to 88.10%) as the pH rose from 7 to 9. The zero-point charge (pH_{ZPC}) was determined to be 7.45. The adsorbent surface becomes positively charged when the solution's pH is lower than pH_{ZPC} and negatively charged when the pH is higher than pH_{ZPC} [65]. This behavior occurs because the extra H^+ ions in the solution cause the adsorbent surface to become protonated at lower pH values ($pH < pH_{ZPC}$). On the other hand, the concentration of OH^- ions in the solution gives the adsorbent surface a negative charge at higher pH values ($pH > pH_{ZPC}$) [66][67].

The NiO (FR) NPs surface becomes protonated at lower pH, which attracts the anionic dye CR and allows dye molecules to stick to the surface. The surface of NiO (FR) NPs becomes negatively charged as the pH rises, repelling anionic dye binding due to increased electrostatic repulsion.

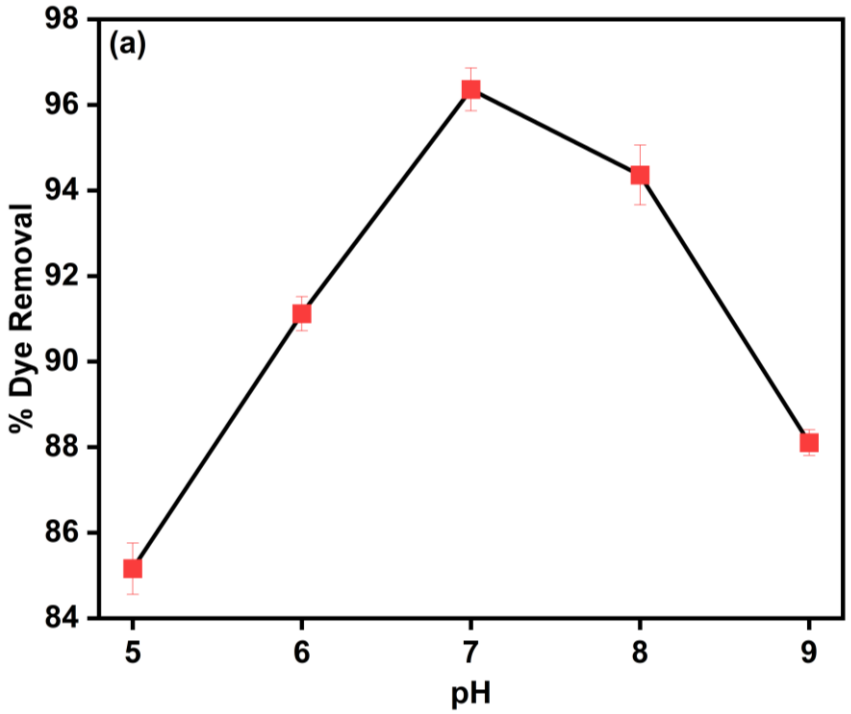
4.3 Probable Mechanism

The mechanism is initially explained by electrostatic attraction and hydrogen bonding (H-bonding) between the cationic surface of the adsorbent and the anionic dye molecules, as presented in Figure 12b. The adsorption of Congo Red to NiO NPs under favorable pH conditions is greatly due to electrostatic attraction between negatively

charged sulfonate groups of Congo Red to the protonated hydroxyl groups of NiO NPs. This is consistent with results showing that NiO NPs are effective for CR removal because their surfaces remain positively charged below the isoelectric point/point of zero charge, which strengthens attraction toward anionic dye molecules.

Furthermore, the total absorption process may also be influenced by secondary interactions such pore filling within the porous NiO structure and hydrogen bonding between surface –OH groups and CR.

In addition, it can be explained based on the surface charge of the synthesized adsorbent, which was calculated using DLS. It was found that NiO (FR) NPs have a potential of 25.2 mV, suggesting strong electrostatic attraction between the positively charged adsorbent and the negatively charged anionic dye molecules.



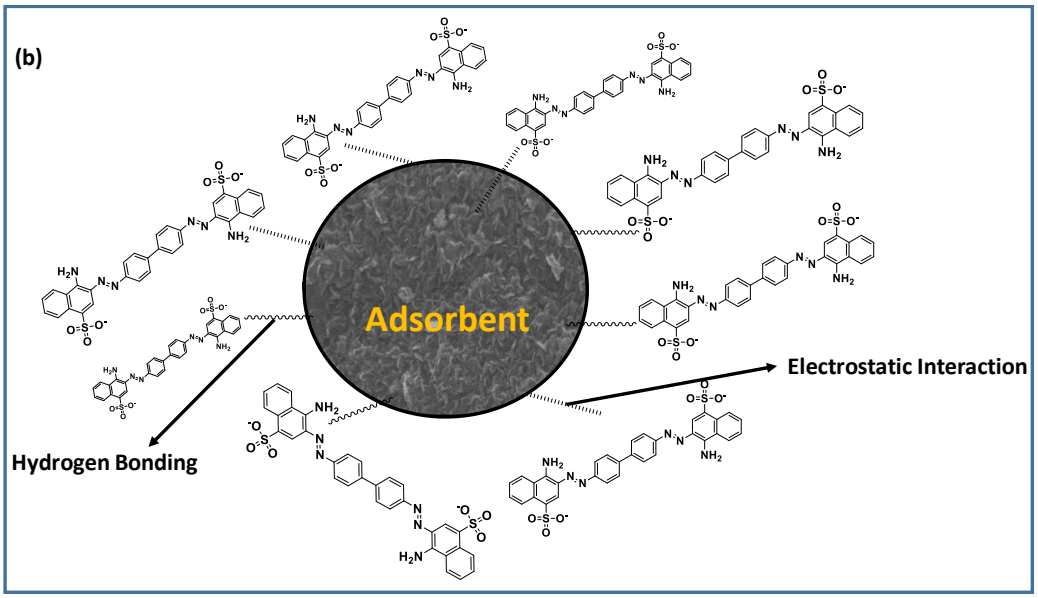


Figure 12. (a) Plots of the effect of pH on dye removal at concentration 30 mg/L, adsorbent dosage 0.1 g, agitating speed 400 rpm, and contact time 25 min, and (b) Plausible mechanism of dye adsorption.

4.4 Kinetics

The kinetic models mentioned above correlated with experimental data to assess the adsorption mechanism. The calculated parameters are shown in Table 1, and the plots in Figure 13 illustrate the linear regression of the experimental data with the kinetic models. The experimental data were found to be in good agreement with the pseudo-first-order model (R^2 = 0.976) for CR, revealing that the rate-determining step in the dye uptake by the designed sorbent. For CR, the value of h was determined to be 0.29 $mg^{-1}min^{-1}$.

Consequently, there are three probable stages to the adsorption of CR on biogenically synthesized NiO (FR) NPs: (i) initial physical sorption, (ii) chemical sorption, and (iii) potential saturation at the equilibrium condition.

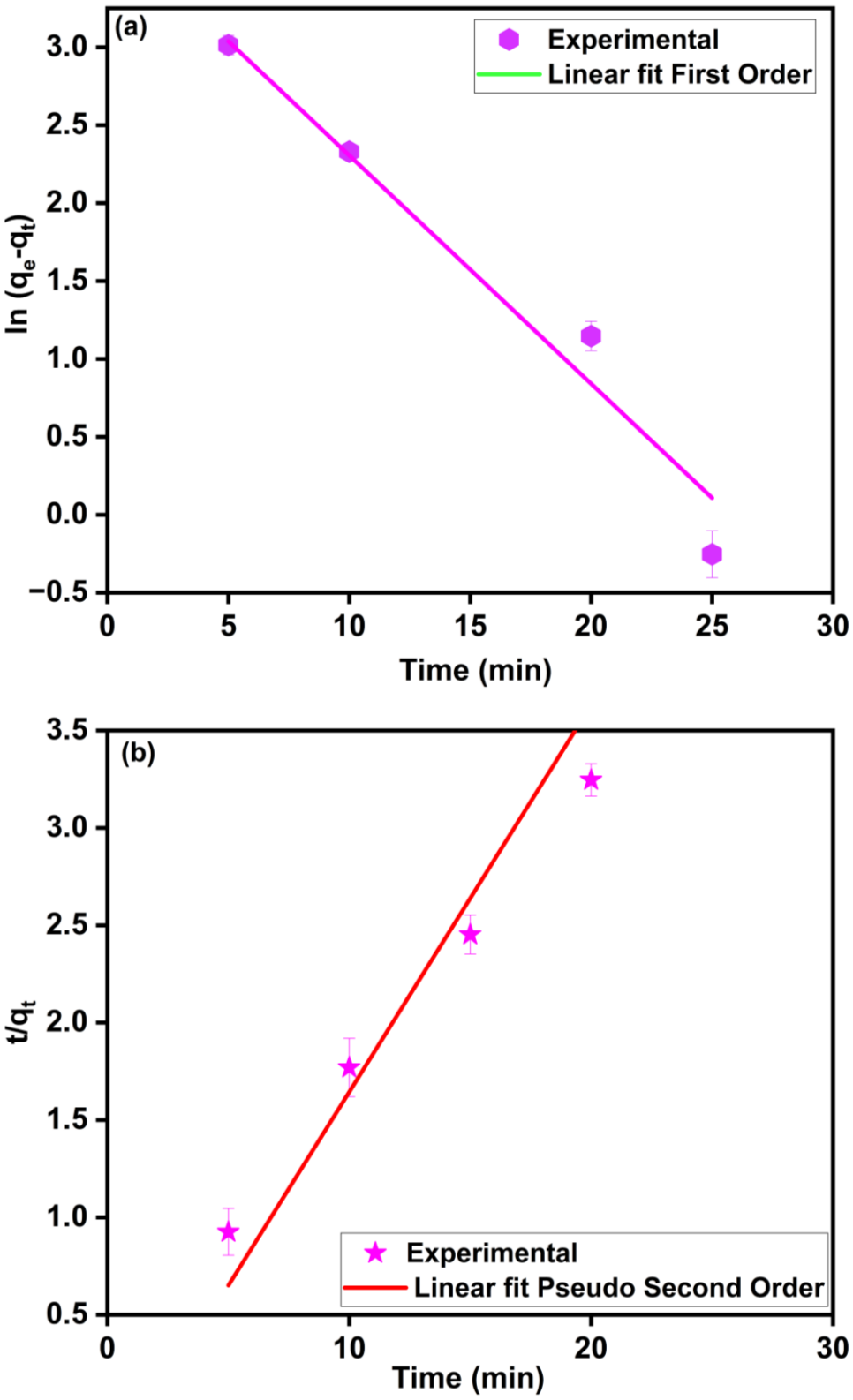


Figure 13. Plots of (a) First order and (b) Pseudo Second Order

Table 1. Calculated Parameters using Both Models.

Kinetics Models Plots	Slope	Intercept	Parameters	Values of Parameters
First order: $\ln(q_e - q_t) = \ln q_e - K_1 t$ K_1 is the rate constant	-0.146	3.77	R^2	0.976
			K_1 (min^{-1})	0.146
			q_e (mg g^{-1})	43.38
Pseudo-second order: $\frac{t}{q_t} = \frac{1}{k_2 q_e^2} + \frac{t}{q_e}$ k_2 is the rate constant $h = k_2 q_e^2$; h is initial adsorption rate	0.198	0.342	R^2	0.963
			K_2 (g mg^{-1} min^{-1})	0.0114
			q_e (mg g^{-1})	5.05
			h (mg g^{-1} min^{-1})	0.29

4.5 Isotherms

The uptake of CR on the NiO (FR) NPs is represented by linear isotherm plots in Figure 14, and the calculated values are shown in Table 2. The linear Langmuir model was found to be in good correlation with the experimental data for the uptake of CR using NiO (FR) NPs, with $R^2 = 0.999$, suggesting homogeneous monolayer adsorption on the adsorbent surface; the R_L was calculated to be 0.0025. The adsorbent's q_{max} was calculated using the Langmuir isotherm, and it was found to be 17 mg g^{-1} for CR (30 mg L^{-1}).

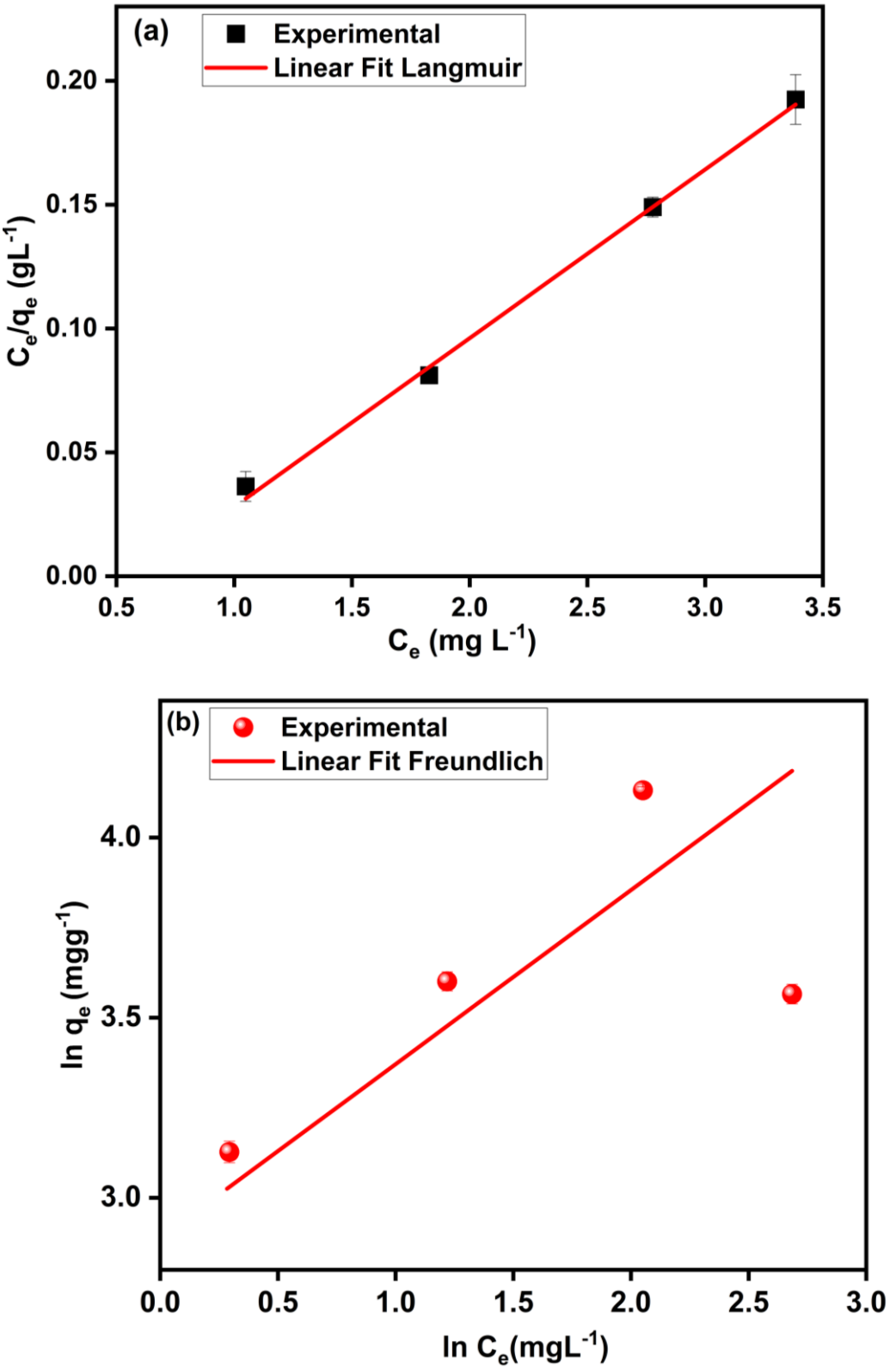


Figure 14. Plot of linear models of (a) Langmuir and (b) Freundlich

Table 2. Calculated Parameters using Various Models.

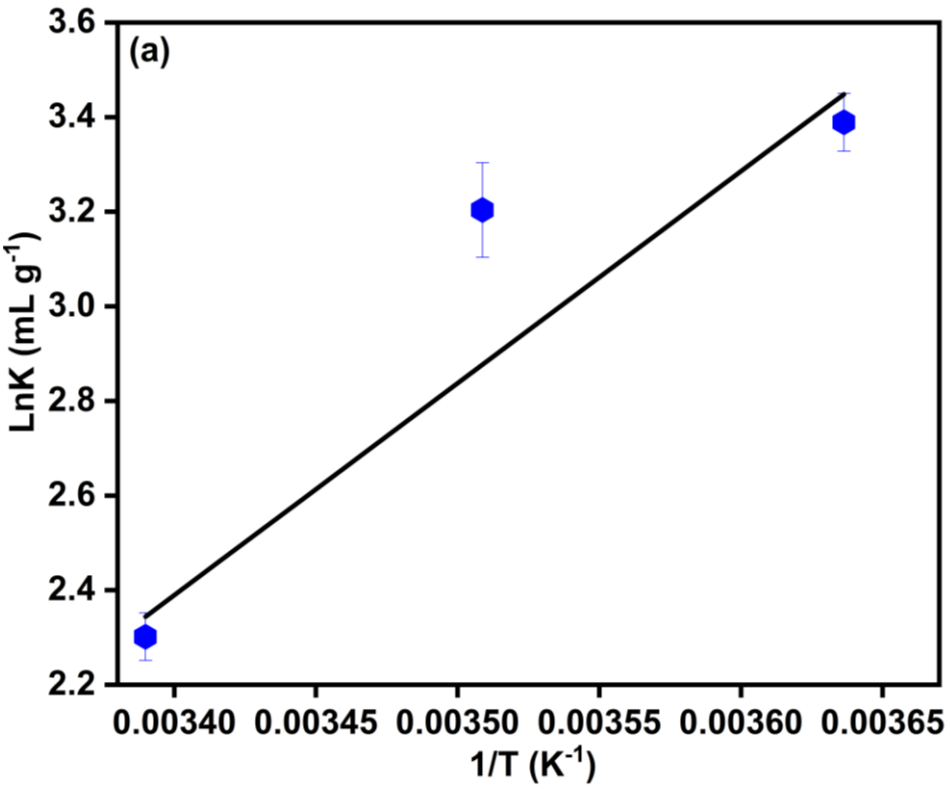
Models	**Slope & Intercept**	**Parameters**	**Computed values**
Langmuir	Slope = 0.06 Intercept =-0.0045	R^2	0.999
		q_m (mg g^{-1})	17
		K_L (L mg^{-1})	13.07
		R_L=1, linearity R_L=0, irreversibility 0 < R_L <1, favourability or un-favourability (RL > 1)	0.0025
Freundlich	Slope = 2.88 Intercept = 4.83	R^2	0.72
		K_F (mg g^{-1}) (L mg)$^{1/n_f}$	73.69
		n_f	0.34

4.6 Thermodynamics

In a study similar to the contact time study, CR dye was adsorption by NiO (FR) NPs at different temperatures (27°C, 37°C, and 47°C). The included parameters, such as enthalpy, entropy, and free energy, were evaluated using the equations presented in Table 3 [68,69].

Temperature plays a crucial role in determining the adsorption capacity of adsorbents. Table 3 and Figure 15. illustrates the equation and the calculated parameter used to determine the thermodynamic parameters of the adsorption process. On the basis of the results, it is concluded that the decrease in sorption efficiency of CR dye on increasing temperature may be the result of weakening absorptive forces between adsorbate and adsorbent, which leads to ions being released and leaching into the liquid, resulting in shrinkage of active sites at higher temperatures [70]. The

thermodynamic parameters indicate that Congo Red adsorption onto the synthesized NiO nanoparticles is spontaneous, as confirmed by the negative ΔG° values. The decrease in the negativity of ΔG° with increasing temperature suggests that the adsorption becomes less favourable at higher temperature, indicating an exothermic process. In addition, the change in enthalpy was negative (-30.15 KJ), suggesting that the sorption was exothermic. Furthermore, the degree of randomness decreased due to the decrease in entropy. Moreover, negative ΔG^0 confirms the feasibility and spontaneous nature of adsorption [69].



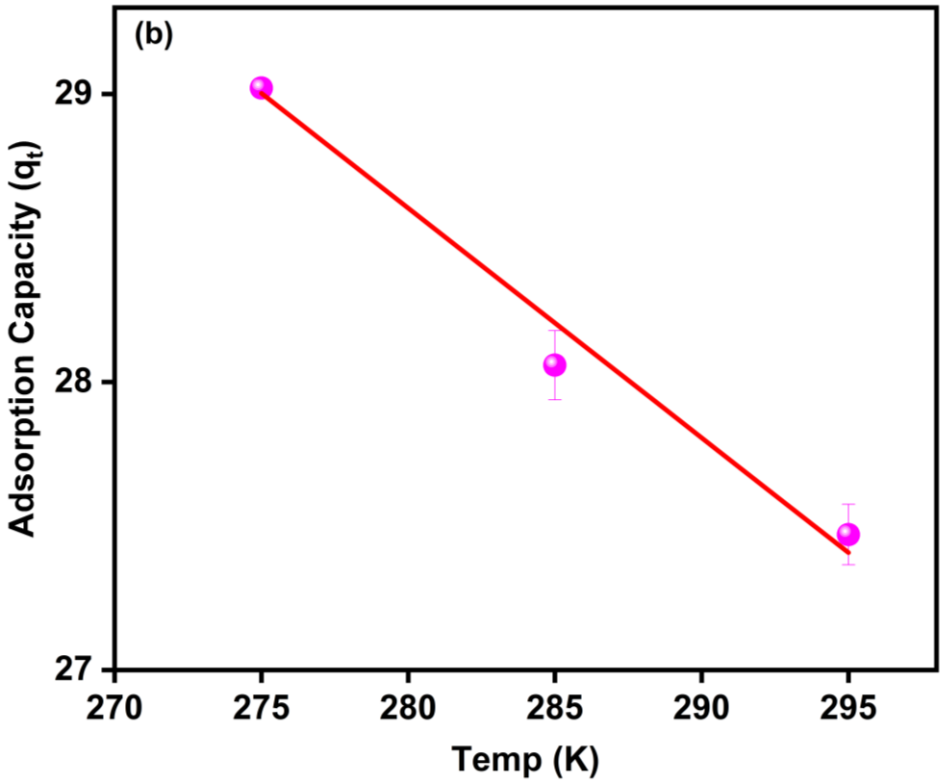


Figure 15. Plot for (a) ln K versus 1/T for CR and (b) impact of temperature on adsorption capacity for CR.

Table 3 Temperature-dependent parameters for CR uptake

Equation used	Temperature (K)	Δ *H* (KJ mol^{-1})	Δ *S*^{o} (J mol^{-1}K^{-1})	Δ *G*^{o} (KJ mol^{-1})
$k_e = \frac{q_e}{C_e}$ $\Delta G^0 = -RT\, ln\, K_e$ $ln\, K_e = \frac{\Delta S^0}{R} - \frac{\Delta H^0}{RT}$	275.15	-30.15	-75.78	-9.068789397
	285.15			-9.016270469
	295.15			-7.553185561

4.7 Regeneration

The regeneration capability of the biosorbent was assessed to ensure reproducibility. To perform the study, batch experiments were conducted [71]. For regeneration of the biosorbent, the biosorbent was collected and cleaned with ethanol and water (1:1) solutions. In the following cycles, the biosorbent was dried at ambient temperatures and used. Based on the data presented in Figure 16a, ~74% dye adsorption was observed at the end of seven cycles. Thus, it is possible to reuse it and to utilize it for remediation of polluted water.

4.8 Different Water Samples

Figure 16b, presented the effectiveness of the synthesized adsorbent for different water samples. Batch adsorption experiment was performed and it was observed that the dye

removal efficacy was more than 80 % even in case of distilled water, suggesting that synthesized adsorbent may consider for practical application in sequestration of dyes.

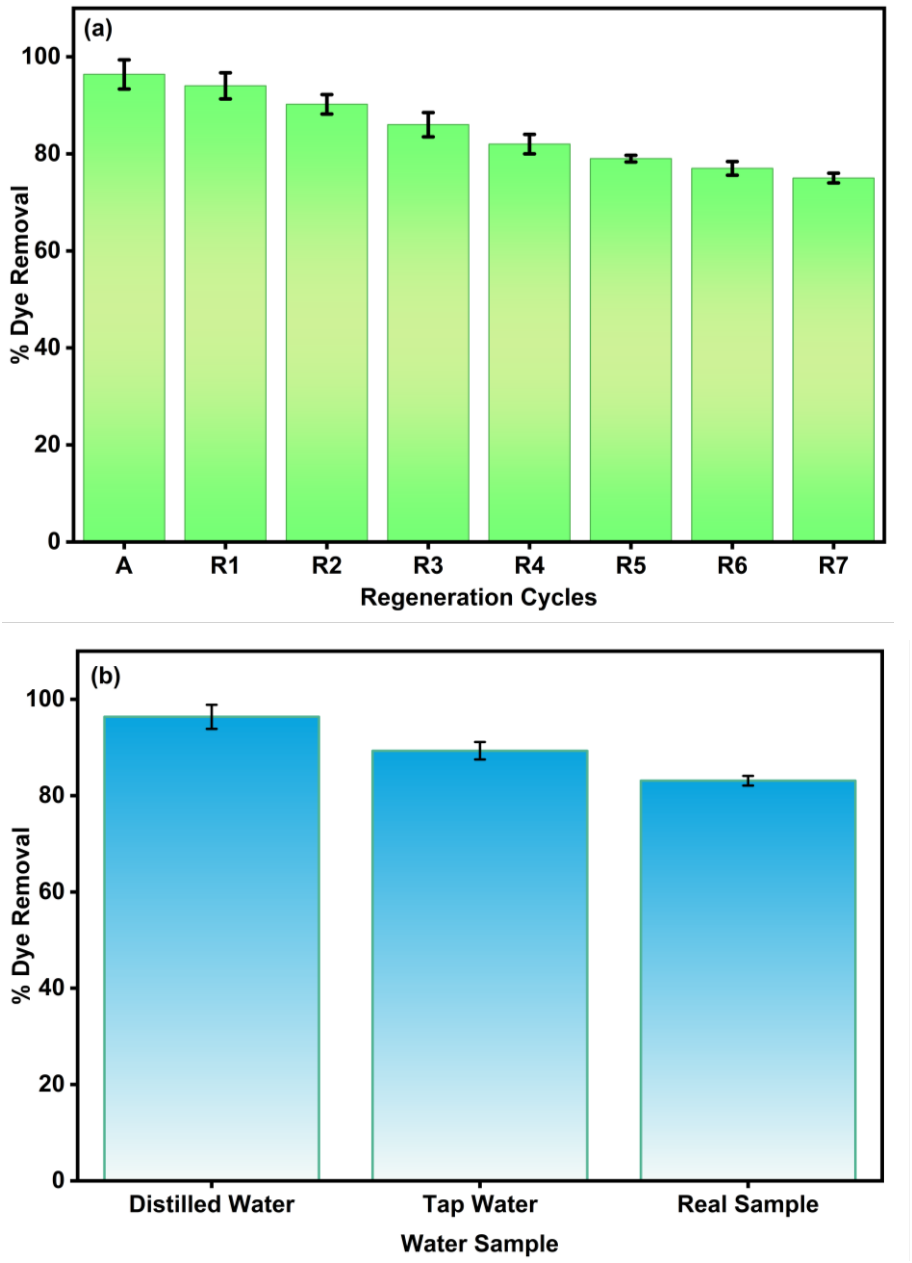


Figure 16. Plot of (a) regeneration cycles of NiO (FR) NPs, and (b) dye removal efficiency from different water sample.

4.9 Comparison with another adsorbent

Table 4. Comparison of synthesized adsorbent with available literature

Material	**% Removal**	**Time**	**Adsorption Capacity (mg/g)**	**Regeneration**	**Reference**
Pd/NiO NPs	86.31	90 min	Moderate adsorption (not quantified as q_{max})	4 cycles	[72]
NiO NPs	93.57	4 h sunlight	-	-	[73]
NiO NPs	56	30 min	Not reported	5 cycles	[73]
ZnO using Brunfelsia americana Leaf Extract	94	250 min	9.39	-	[74]
CuO from Malva sylvestris	~80	30 min	6.99	4	[75]
NiO (FR) NPs	**96.36**	**25 min**	**17**	**Efficient after 7 cycles**	**Present Work**

CHAPTER 5

CONCLUSION

The FR plant is the source of stabilizing and capping agent in this study. These leaves were used to synthesized NiO (FR) NPs as a biosorbent to sequestrate CR dye from synthetic aqueous wastewater. The adsorption process is supported by active surface area was also computed and found to be higher (44.721 m^2/g) in NiO (FR) NPs and lesser (33.902 m^2/g) in activated NiO NPs (control), indicating that NiO (FR) NPs is better for adsorption. After examining the effects of several factors, including concentration and contact time, it was found that approximately 96.36% of the CR dye could be removed from aqueous media in just 25 minutes. It was discovered that the highest adsorption capacity was 17 mg/g. Further, isotherm and kinetic studies were performed, which revealed that sorbent follows monolayer adsorption (R^2= 0.999) and pseudo-first-order (R^2 = 0.98). The temperature studies showed exothermic nature of the adsorbent. In addition to that, regeneration studies were also performed, and it was found that the sorbent efficiently adsorbs CR dye after 5 cycles. Hence, the sorbent can be used in practical importance.

References

[1] H. Sadiq, F. Sher, S. Sehar, E.C. Lima, S. Zhang, H.M.N. Iqbal, F. Zafar, M. Nuhanović, Green synthesis of ZnO nanoparticles from Syzygium Cumini leaves extract with robust photocatalysis applications, J. Mol. Liq. 335 (2021). https://doi.org/10.1016/j.molliq.2021.116567.

[2] J.K.H. Wong, K.K. Lee, K.H.D. Tang, P.S. Yap, Microplastics in the freshwater and terrestrial environments: Prevalence, fates, impacts and sustainable solutions, Sci. Total Environ. 719 (2020) 137512. https://doi.org/10.1016/j.scitotenv.2020.137512.

[3] S. Lai, Y. Jin, L. Shi, Y. Li, R. Zhou, Tailoring multifunctional gel for sensitive naked-eye and fluorescence dual-mode detection and effective adsorption of cadmium(II) and lead(II) ions in water, Chem. Eng. J. 429 (2022) 132367. https://doi.org/10.1016/j.cej.2021.132367.

[4] X. Ma, X. Wang, X. Yin, X. Kan, Z. Wang, Electrochemical stripping of cotton fabrics dyed with Reactive Black 5 in water and wastewater, Chemosphere 206 (2018) 17–25. https://doi.org/10.1016/j.chemosphere.2018.04.122.

[5] A. Salar, F. Kiani, N. Rezaee, Preventing the medication errors in hospitals: A qualitative study, Int. J. Africa Nurs. Sci. 13 (2020) 100235. https://doi.org/10.1016/j.ijans.2020.100235.

[6] T.M. Evans, L. Bira, J.B. Gastelum, L.T. Weiss, N.L. Vanderford, Evidence for a mental health crisis in graduate education, Nat. Biotechnol. 36 (2018) 282–284. https://doi.org/10.1038/nbt.4089.

[7] A. Grover, I. Mohiuddin, A.K. Malik, J.S. Aulakh, Adsorption studies of organic dyes on surfactant modified Zn-Al layered double hydroxide, (2020). https://doi.org/10.13140/RG.2.2.10003.71202.

[8] P. Yadav, K. Kashyap, S.G. Warkar, A. Kumar, FeO NPs-Loaded Guar Gum / Xanthan Gum-Based Hydrogel : A Sustainable Approach for Cationic Dye Removal, ChemistrySelect 10 (2025) 1–16. https://doi.org/10.1002/slct.202500293.

[9] P. Debnath, N.K. Mondal, Effective removal of congo red dye from aqueous solution using biosynthesized zinc oxide nanoparticles, Environ. Nanotechnology, Monit. Manag. 14 (2020) 100320. https://doi.org/10.1016/j.enmm.2020.100320.

[10] R. Nodehi, H. Shayesteh, A.R. Kelishami, Enhanced adsorption of congo red using cationic surfactant functionalized zeolite particles, Microchem. J. 153

(2020) 104281. https://doi.org/10.1016/j.microc.2019.104281.

[11] H. Shayesteh, A. Rahbar-Kelishami, R. Norouzbeigi, Evaluation of natural and cationic surfactant modified pumice for congo red removal in batch mode: Kinetic, equilibrium, and thermodynamic studies, J. Mol. Liq. 221 (2016) 1–11. https://doi.org/10.1016/j.molliq.2016.05.053.

[12] G.M. Galvani, C.A. Zito, T.M. Perfecto, J.O.D. Malafatti, E.C. Paris, D.P. Volanti, Two-dimensional NiO nanosheets for efficient Congo red adsorption removal, Mater. Chem. Phys. 290 (2022) 126591. https://doi.org/10.1016/j.matchemphys.2022.126591.

[13] L.S. Alqarni, M.N. Goda, M.Q. Alfaifi, M. Aleid, A.H. Ahmed, A. Alsulami, A. Modwi, Congo red eradication via efficient La-NiO-g-C3N4 nanocomposite from contaminated water, J. Hazard. Mater. Adv. 18 (2025) 100751. https://doi.org/10.1016/j.hazadv.2025.100751.

[14] H.C.T. Firmino, E.P. Nascimento, K.C. Costa, L.C.C. Arzuza, R.N. Araujo, B. V. Sousa, G.A. Neves, M.A. Morales, R.R. Menezes, High-Efficiency Adsorption Removal of Congo Red Dye from Water Using Magnetic NiFe2O4 Nanofibers: An Efficient Adsorbent, Materials (Basel). 18 (2025) 1–17. https://doi.org/10.3390/ma18040754.

[15] D. Sharma, L. Sharma, Phytochemistry and therapeutic applications of Ficus religiosa: A comprehensive review, Phytochem. Lett. 71 (2026). https://doi.org/10.1016/j.phytol.2025.104096.

[16] P.J. Wang, X.P. Hu, D.J. Liao, Y. Wen, T.R. Hull, F. Miao, Q.T. Zhang, Dual fire retardant action: The combined gas and condensed phase effects of azo-modified NiZnAl layered double hydroxide on intumescent polypropylene, Ind. Eng. Chem. Res. 56 (2017) 920–932. https://doi.org/10.1021/acs.iecr.6b03953.

[17] S. Pandey, N. Son, S. Kim, D. Balakrishnan, M. Kang, Locust Bean gum-based hydrogels embedded magnetic iron oxide nanoparticles nanocomposite: Advanced materials for environmental and energy applications, Environ. Res. 214 (2022) 114000. https://doi.org/10.1016/j.envres.2022.114000.

[18] E. Pournamdari, L. Niknam, S. Davoudi, F. Khazali, Response surface methodology , and artificial neural network model for removal of textile dye Reactive Yellow 105 from wastewater using Zeolitic Imidazolate-67 modified by Fe 3 O 4 nanoparticles Response surface methodology , and artificial neural network, Int. J. Phytoremediation 26 (2024) 98–113. https://doi.org/10.1080/15226514.2023.2226217.

[19] P. Yadav, S.G. Warkar, A. Kumar, Development of graphene oxide-incorporated biopolymer-carboxymethyl tamarind kernel gum-based hydrogel

as an effective adsorbent for the sequestration of dye pollutants, Polym. Eng. Sci. 64 (2024) 1–18. https://doi.org/10.1002/pen.26883.

[20] S. Pandey, S. Kim, Y.S. Kim, D. Kumar, M. Kang, Fabrication of next-generation multifunctional LBG-s-AgNPs@ g-C3N4 NS hybrid nanostructures for environmental applications, Environ. Res. 240 (2024) 117540. https://doi.org/10.1016/j.envres.2023.117540.

[21] P. Yadav, S.G. Warkar, A. Kumar, Application of nanomaterials in water purification, in: Nanotechnol. A Quick Guid. to Mater. Technol., 2024: pp. 254–295. https://doi.org/10.2174/9789815256772124010011.

[22] V. Katheresan, J. Kansedo, S.Y. Lau, Efficiency of various recent wastewater dye removal methods: A review, J. Environ. Chem. Eng. 6 (2018) 4676–4697. https://doi.org/10.1016/j.jece.2018.06.060.

[23] A. Jaiswal, R.K. Gautam, M.C. Chattopadhyaya, Layered Double Hydroxides and the Environment: An Overview, Adv. Mater. Agric. Food Environ. Saf. 9781118773 (2014) 1–26. https://doi.org/10.1002/9781118773857.ch1.

[24] M. Afzaal, R. Nawaz, S. Hussain, M. Nadeem, M.A. Irshad, A. Irfan, H.A. Mannan, A.A. Al Mutairi, A. Islam, S.A. Al Hussain, M. Rubab, M.E.A. Zaki, Removal of oxytetracycline from pharmaceutical wastewater using kappa carrageenan hydrogel, Sci. Rep. (2024) 1–14. https://doi.org/10.1038/s41598-024-69989-x.

[25] S.R. Mukai, H. Nishihara, S. Shichi, H. Tamon, Preparation of porous TiO2 cryogel fibers through unidirectional freezing of hydrogel followed by freeze-drying, Chem. Mater. 16 (2004) 4987–4991. https://doi.org/10.1021/cm0491328.

[26] R. Geetha, Hybrid Synthesis Strategies of NiO Nanostructures for Photocatalytic Dye Removal from Contaminated Water Sources: A Critical Review, Hybrid Adv. 12 (2026) 100601. https://doi.org/10.1016/j.hybadv.2026.100601.

[27] I. Seete, D.A. Bopape, L.M. Mahlaule-Glory, Z. Tetana, N.C. Hintsho-Mbita, Plant-Mediated Synthesis of NiO Nanoparticles for Textile Dye Degradation in Water: A Review, Colorants 4 (2025) 7. https://doi.org/10.3390/colorants4010007.

[28] M.A. Kiser, P. Westerhoff, T. Benn, Y. Wang, J. Pérez-Rivera, K. Hristovski, Titanium nanomaterial removal and release from wastewater treatment plants, Environ. Sci. Technol. 43 (2009) 6757–6763. https://doi.org/10.1021/es901102n.

[29] H. Chemingui, S. Rezma, R. Lafi, Z. Alhalili, T. Missaoui, I. Harbi, M. Smiri,

A. Hafiane, Investigation of methylene blue adsorption from aqueous solution onto ZnO nanoparticles : equilibrium and Box-Behnken optimisation design solution onto ZnO nanoparticles : equilibrium and Box-, Int. J. Environ. Anal. Chem. 103 (2023) 2716–2741. https://doi.org/10.1080/03067319.2021.1897121.

[30] H. Chemingui, R. Lafi, T. Missaoui, I. Montasser, A. Hafiane, M. Kamoun, Eco-friendly approach for the synthesis of zinc oxide nanoparticles (ZnO NPs) using Verbena officinalis L: enhancement of photocatalytic activity under UV light and application of response surface methodology, Biomass Convers. Biorefinery 15 (2025) 4281–4299. https://doi.org/10.1007/s13399-024-05549-7.

[31] Y. Ahmadian, A. Bakravi, H. Hashemi, H. Namazi, Synthesis of polyvinyl alcohol/CuO nanocomposite hydrogel and its application as drug delivery agent, Polym. Bull. 76 (2019) 1967–1983. https://doi.org/10.1007/s00289-018-2477-9.

[32] A.N.R. Leal, L.B.C. de Oliveira, A. da C.A. de Lima, M.F. de Aguiar, J. Silva, I.J. da C. Filho, Remazol Red dye removal in water solutions using a mixed adsorvent composed of Aspergillus Niger and Elephant Grass, Rev. Gestão Sustentabilidade Ambient. 10 (2021) 358–376.

[33] N. Beigi, H. Shayesteh, S. Javanshir, M. Hosseinzadeh, Pyrolyzed magnetic NiO/carbon-derived nanocomposite from a hierarchical nickel-based metal-organic framework with ultrahigh adsorption capacity, Environ. Res. 231 (2023) 116146. https://doi.org/10.1016/j.envres.2023.116146.

[34] F.M. Mohamed, A.M. Alfalos, M.F. Alrakshy, M.A. Aborziza, K.A. Alfalous, M.A. Rafea, M.E.A. Zaki, M.R. El-Aassar, M.A. Roshdy, Sustainable removal of azo dyes from real effluents using a biomass-derived composite, Sci. Rep. 16 (2026) 1–23. https://doi.org/10.1038/s41598-025-32434-8.

[35] A. Berhe, F. Tilahun, A. Wendu, W. Lakew, Plant-mediated biosynthesis of Nickel (II) oxide nanoparticles from Calpurnia Aurea Leaf extract: A promising photocatalyst for malachite green degradation, Chem. Phys. Impact 11 (2025) 100906. https://doi.org/10.1016/j.chphi.2025.100906.

[36] H.A. Al-aoh, Adsorption performances of nickel oxide nanoparticles (NiO NPs) towards bromophenol blue dye (BB) Adsorption performances of nickel oxide nanoparticles (NiO NPs) towards bromophenol blue dye (BB), (2018). https://doi.org/10.5004/dwt.2018.22223.

[37] A. Miri, F. Mahabbati, A. Najafidoust, J. Miri, M. Sarani, Nickel oxide nanoparticles : biosynthesized , characterization and photocatalytic application in degradation of methylene blue dye, Inorg. Nano-Metal Chem. 0 (2020) 1–10. https://doi.org/10.1080/24701556.2020.1862226.

[38] K.G. Akpomie, S. Ghosh, M. Gryzenhout, J. Conradie, One-pot synthesis of zinc oxide nanoparticles via chemical precipitation for bromophenol blue adsorption and the antifungal activity against filamentous fungi, Sci. Rep. 11 (2021) 1–17. https://doi.org/10.1038/s41598-021-87819-2.

[39] M.S. Amir Faiz, C.A. Che Azurahanim, S.A. Raba'ah, M.Z. Ruzniza, Low cost and green approach in the reduction of graphene oxide (GO) using palm oil leaves extract for potential in industrial applications, Results Phys. 16 (2020) 102954. https://doi.org/10.1016/j.rinp.2020.102954.

[40] U. Dalal, S.N. Reddy, A novel nano zero-valent iron biomaterial for chromium (Cr 6+ to Cr 3+) reduction, Environ. Sci. Pollut. Res. 26 (2019) 10631–10640. https://doi.org/10.1007/s11356-019-04528-0.

[41] Y. Subba Reddy, N.K. Rotte, B.K. Sudhakar, N. Ramakrishna Chand, R.J. Naik, S. Mandal, M. Ravi Chandra, Biomass-derived sustainable mesoporous activated carbon as an efficient and recyclable adsorbent for the adsorption of hazardous dyes, Hybrid Adv. 6 (2024) 100218. https://doi.org/10.1016/j.hybadv.2024.100218.

[42] Z. Mohamed Riyas, R. Gayathri, M.R. Prabhu, K. Velsankar, S. Sudhahar, Green synthesis and biomedical behavior of Mg-doped ZnO nanoparticle using leaf extract of Ficus religiosa, Ceram. Int. 48 (2022) 24619–24628. https://doi.org/10.1016/j.ceramint.2022.05.107.

[43] J. Sukumaran, M. Priya, R. Venkatesan, K. Sathiasivan, M.R. Khan, S.C. Kim, Green Synthesis of Nickel Oxide Nanoparticles Using Leaf Extract of Aegle marmelos and Their Antibacterial, Anti-Oxidant, and In Vitro Cytotoxicity Activity, Microsc. Res. Tech. 88 (2025) 2830–2842. https://doi.org/10.1002/jemt.70054.

[44] S.M. Ghoreishi, S. Mortazavi-Derazkola, Eco-friendly synthesis of gold nanoparticles via tangerine peel extract: Unveiling their multifaceted biological and catalytic potentials, Heliyon 11 (2025) e40104. https://doi.org/10.1016/j.heliyon.2024.e40104.

[45] P. Patel, I. Dimitriou, P. Mondal, O. Singh, S. Gupta, Process optimisation and enviro-economic assessment of carbon-negative hydrogen production from biomass co-gasification, Energy Convers. Manag. 323 (2025) 119211. https://doi.org/10.1016/j.enconman.2024.119211.

[46] S. Kalam, S.A. Abu-khamsin, M.S. Kamal, S. Patil, Surfactant Adsorption Isotherms : A Review, (2021). https://doi.org/10.1021/acsomega.1c04661.

[47] M. Musah, Y. Azeh, J. Mathew, M. Umar, Z. Abdulhamid, A. Muhammad, Adsorption Kinetics and Isotherm Models: A Review, Caliphate J. Sci.

Technol. 4 (2022) 20–26. https://doi.org/10.4314/cajost.v4i1.3.

[48] J.C. Bullen, S. Saleesongsom, K. Gallagher, D.J. Weiss, A Revised Pseudo-Second-Order Kinetic Model for Adsorption, Sensitive to Changes in Adsorbate and Adsorbent Concentrations, Langmuir 37 (2021) 3189–3201. https://doi.org/10.1021/acs.langmuir.1c00142.

[49] N. Ayawei, A.N. Ebelegi, D. Wankasi, Modelling and Interpretation of Adsorption Isotherms, J. Chem. 2017 (2017). https://doi.org/10.1155/2017/3039817.

[50] H. Freundlich, Über die Adsorption in Lösungen, Zeitschrift Für Phys. Chemie 57U (1907) 385–470. https://doi.org/10.1515/zpch-1907-5723.

[51] P. Yadav, S.G. Warkar, A. Kumar, Fabrication of carboxymethyl tamarind kernel gum-based pH-responsive hydrogel composite for oral delivery of azithromycin drug, Int. J. Biol. Macromol. 322 (2025) 146662. https://doi.org/10.1016/j.ijbiomac.2025.146662.

[52] N.A. Yahya, R. Abdul Wahab, N. Attan, M. Abdul Hamid, N. Mohamed Noor, R. Kobun, Ananas comosus Peels Extract as a New Natural Cosmetic Ingredient: Oil-in-Water (O/W) Topical Nano Cream Stability and Safety Evaluation, Evidence-Based Complement. Altern. Med. 2022 (2022). https://doi.org/10.1155/2022/2915644.

[53] Z. Sun, L. Wang, X. Jiang, L. Bai, W. Wang, H. Chen, L. Yang, H. Yang, D. Wei, Self-healing, sensitive and antifreezing biomass nanocomposite hydrogels based on hydroxypropyl guar gum and application in flexible sensors, Int. J. Biol. Macromol. 155 (2020) 1569–1577. https://doi.org/10.1016/j.ijbiomac.2019.11.134.

[54] S. Dey, R. Chakraborty, J. Mohanta, B. Dey, Tricosanthes cucumerina: a potential biomass for efficient removal of methylene blue from water, Bioremediat. J. 0 (2022) 1–15. https://doi.org/10.1080/10889868.2022.2086530.

[55] R. Kaur, H. Kaur, Calotropis procera an effective adsorbent for removal of Congo red dye: isotherm and kinetics modelling, Model. Earth Syst. Environ. 3 (2017) 1–13. https://doi.org/10.1007/s40808-017-0274-3.

[56] P. Nikolaidis, A. Poullikkas, A comparative overview of hydrogen production processes, Renew. Sustain. Energy Rev. 67 (2017) 597–611. https://doi.org/10.1016/j.rser.2016.09.044.

[57] S. Prabhu, T. Daniel Thangadurai, P. Vijai Bharathy, P. Kalugasalam, Synthesis and characterization of nickel oxide nanoparticles using Clitoria ternatea flower extract: Photocatalytic dye degradation under sunlight and

antibacterial activity applications, Results Chem. 4 (2022) 100285. https://doi.org/10.1016/j.rechem.2022.100285.

[58] P. Vijaya Kumar, A. Jafar Ahamed, M. Karthikeyan, Synthesis and characterization of NiO nanoparticles by chemical as well as green routes and their comparisons with respect to cytotoxic effect and toxicity studies in microbial and MCF-7 cancer cell models, SN Appl. Sci. 1 (2019). https://doi.org/10.1007/s42452-019-1113-0.

[59] S. Chakrabarty, K. Chatterjee, Synthesis and Characterization of Nano-Dimensional Nickelous Oxide (NiO) Semiconductor, J. Phys. Sci. 13 (2009) 245–250.

[60] J.O. Quansah, T. Hlaing, F.N. Lyonga, P.P. Kyi, S.H. Hong, C.G. Lee, S.J. Park, Nascent rice husk as an adsorbent for removing cationic dyes from textile wastewater, Appl. Sci. 10 (2020). https://doi.org/10.3390/app10103437.

[61] N. Singh, S. Riyajuddin, K. Ghosh, S.K. Mehta, A. Dan, Chitosan-Graphene Oxide Hydrogels with Embedded Magnetic Iron Oxide Nanoparticles for Dye Removal, ACS Appl. Nano Mater. 2 (2019) 7379–7392. https://doi.org/10.1021/acsanm.9b01909.

[62] N.A. Hussain, A. Taifi, O.K.A. Alkadir, N.H. Obaid, Z.M. Abboud, A.M. Aljeboree, A.L. Al Bayaa, S.A. Abed, A.F. Alkaim, Role of Pomegranate peels as a activated carbon for removal of pollutants, IOP Conf. Ser. Earth Environ. Sci. 1029 (2022). https://doi.org/10.1088/1755-1315/1029/1/012028.

[63] J. Pathak, P. Singh, Adsorptive Removal of Congo Red Using Organically Modified Zinc–Copper–Nickel Ternary Metal Hydroxide: Kinetics, Isotherms and Adsorption Studies, J. Polym. Environ. 31 (2023) 327–344. https://doi.org/10.1007/s10924-022-02612-0.

[64] A. Jangir, P.P. Samal, A.K. Jangir, B. Dey, S. Dey, Exploring Ficus religiosa inflorescence powder as an eco-friendly and sustainable solution for the removal of crystal violet with a disposal solution, Environ. Monit. Assess. 196 (2024) 728. https://doi.org/10.1007/s10661-024-12866-x.

[65] K.G. Akpomie, J. Conradie, Efficient adsorptive removal of paracetamol and thiazolyl blue from polluted water onto biosynthesized copper oxide nanoparticles, Sci. Rep. 13 (2023) 1–16. https://doi.org/10.1038/s41598-023-28122-0.

[66] M. Kizilyalli, Solid-state chemistry: review and development of teaching materials and definition of terms, IUPAC Congr. (2001) 10 pp. http://scholar.google.com/scholar?hl=en&btnG=Search&q=intitle:SOLID-STATE+CHEMISTRY+Review+and+development+of+teaching+materials+and+definition+of+terms#7.

[67] A.A.E.A. Elfiky, M.F. Mubarak, M. Keshawy, I.E.T. El Sayed, T.A. Moghny, Novel nanofiltration membrane modified by metal oxide nanocomposite for dyes removal from wastewater, Environ. Dev. Sustain. 26 (2024) 19935–19957. https://doi.org/10.1007/s10668-023-03444-1.

[68] H.A.S. Tohamy, M. El-Sakhawy, S. Kamel, Development of Magnetite/Graphene Oxide Hydrogels from Agricultural Wastes for Water Treatment, J. Renew. Mater. 10 (2022) 1889–1909. https://doi.org/10.32604/jrm.2022.019211.

[69] B. Pandey, P. Singh, Statistical Optimization of Process Parameters for Ultrafast Uptake of Anionic Azo Dyes by Efficient Sorbent: Zn/Cu Layered Double Hydroxide, Appl. Organomet. Chem. (2023) 1–18. https://doi.org/10.1002/aoc.7072.

[70] R.A. Anayurt, A. Sari, M. Tuzen, Equilibrium, thermodynamic and kinetic studies on biosorption of Pb(II) and Cd(II) from aqueous solution by macrofungus (Lactarius scrobiculatus) biomass, Chem. Eng. J. 151 (2009) 255–261. https://doi.org/10.1016/j.cej.2009.03.002.

[71] P. Yadav, Rachana, V. Jha, Divyanshu, S.G. Warkar, A. Kumar, Harnessing alkali assisted Calotropis gigantea leaf as phytosorbent for removal of crystal violet from water, Int. J. Phytoremediation (2025). https://doi.org/10.1080/15226514.2025.2533522.

[72] O.I. Omotunde, E. Gurgur, A.M. Ojo, O.M. Abiodun, A.E. Okoronkwo, Oxidant-assisted catalytic degradation of Congo red by Pd/NiO nanoparticles under visible light, Acad. Eng. 2 (2025) 1–11. https://doi.org/10.20935/acadeng7542.

[73] S.R. Shakor, S.T. Fardood, A. Naghipour, Green synthesis and characterization of NiO nanoparticles with enhanced sonocatalytic activity, Iran. J. Catal. 15 (2025) 1–10. https://doi.org/10.57647/j.ijc.2025.1503.30.

[74] M.R. Akanda, M.F. Hasan, M. Al-Amin, Green Synthesis and Characterization of ZnO Nanoparticles Using Brunfelsia americana Leaf Extract: Isotherm, Kinetics, Thermodynamic Insights and Reusability into Malachite Green Dye Removal from Aqueous Solutions, South African J. Chem. Eng. 55 (2026) 11–23. https://doi.org/10.1016/j.sajce.2025.10.001.

[75] A.J.M. Ameen, K.M. Omer, A.K. Qasim, Enhanced adsorption of an organic dye by phyto-synthesized CuO nanoparticles derived from Malva sylvestris for sustainable environmental remediation , Mater. Adv. 6 (2025) 8139–8156. https://doi.org/10.1039/d5ma00697j.

INTERNATIONAL JOURNAL OF PHYTOREMEDIATION
https://doi.org/10.1080/15226514.2026.2674242

Taylor & Francis
by Informa

Check for updates

Biogenic synthesis of NiO nanoparticles using *Ficus religiosa* and their application to sequestrate anionic dye

Priyanka Yadav, Jyoti Tomar, Harshita Thapa, Sudhir G. Warkar, and Anil Kumar

Department of Applied Chemistry, Delhi Technological University, Delhi, India

ABSTRACT

This study demonstrates the use of *Ficus religiosa* (FR) leaves as a natural, cost-effective, green stabilizing and capping agent for the synthesis of nickel oxide (NiO) nanoparticles (NPs) for the sequestration of anionic Congo Red (CR). Various techniques, including FTIR, XRD, field-emission scanning electron microscopy, dynamic light scattering, Brunauer–Emmett–Teller, HRTEM, and a UV–Vis spectrophotometer, were employed to demonstrate the efficiency of the synthesized NiO (FR) NPs as a biosorbent. The crystallite size of the NPs was found to be 5 nm for NiO NPs (control) and 2.8 nm for Ni (FR) NPs, calculated using XRD. The adsorption behavior of the biosorbent was examined by varying several parameters, such as pH, dye concentration, adsorbent amount, and equilibrium time. Adsorption isotherms and kinetic models were also fitted. The maximum adsorption capacity of CR on biogenically synthesized NiO NPs was found to be 17 mg g^{-1}, achieved at 37°C or 310.15 K. Isotherm and kinetic studies revealed that Langmuir and pseudo-first order were found to be the best fit. The recyclability of the adsorbent remains good after 5 cycles of regeneration, with the adsorbent achieving ~83% removal using the real wastewater sample. Overall, NiO (FR) NPs, as a sorbent based on dried FR leaves, exhibit strong potential as an effective biosorbent for the adsorption of CR *via* contaminated water.

KEYWORDS

Anionic dye; biomass; biosorbent; *Ficus religiosa*; sequestration

NOVELTY STATEMENT

In this study, waste leaves of *Ficus religiosa* (FR), commonly known as peepal, an indigenous plant. The leaves were used as a green reducing and stabilizing agent for the synthesis of nickel oxide (NiO) nanoparticles (NPs). The synthesized NiO NPs were then applied for the removal of Congo Red (CR) dye from aqueous solution through batch adsorption experiments.

To the best of our knowledge, no previous study has reported the green synthesis of NiO NPs using FR waste leaves specifically for the sequestration of CR. The FR-mediated NiO NPs exhibited good removal performance compared with conventionally synthesized control NiO NPs, mainly due to their higher surface area and improved water stability. These properties make the synthesized nanomaterial efficient for anionic dye removal. Therefore, this work presents a novel, eco-friendly, facile, and potentially scalable alternative to conventional and costly adsorbents. This approach introduces a novel, eco-friendly, green, facile, and scalable alternative to conventional and more expensive adsorbents. It highlights its potential for real-world wastewater treatment applications.

GRAPHICAL ABSTRACT



Introduction

Currently, globally, industrial effluents, agricultural runoff, and municipal wastewater are the primary sources of water pollution, posing a significant threat to flora and fauna (Sadiq *et al.* 2021). Freshwater systems are under tremendous strain due to increased industrialization, urbanization,

CONTACT Anil Kumar anil_kumar@dce.ac.in Department of Applied Chemistry, Delhi Technological University, Delhi 110042, India.
© 2026 Taylor & Francis Group, LLC